ON THE OPTIMUM DESIGN OF THE CORNER ARRAY

by

HASSAN A. RAGHEB

A thesis
presented to the University of Manitoba
in partial fulfillment of the
requirements for the degree of
Master of Science
in
Electrical Engineering

Winnipeg, Manitoba, 1984

ON THE OPTIMUM DESIGN OF THE CORNER ARRAY

by

Hassan A. Ragheb

A thesis submitted to the Faculty of Graduate Studies of the University of Manitoba in partial fulfillment of the requirements of the degree of

MASTER OF SCIENCE

ABSTRACT

The thesis describes an optimization of Schell's design of the corner array in order to take into account the edge diffraction, mutual coupling, and off-axis positioning of the radiators, as well as arbitrary corner angles.

Initially, an optimization procedure for generating partial optimum pattern and optimum gain has been given for each effect separately. Analysis of the off-axis symmetrical or asymmetrical positioning of the radiators is given. The mutual coupling between the radiators and between the reflector surfaces and the radiators are investigated separately. The effect of edge diffraction on the radiation characteristics is also investigated using the integral equation formulation and the geometrical theory of diffraction.

Finally, an example is presented to illustrate how all effects can be taken into account simultaneously in order to yield a global optimum which satisfies specifice design characteristics. It is shown that for the specific case of the unequispaced corner array treated by Schell, the resulting improvements with respect to the gain and main to sidelobe ratio are 2.67 dB and 2.6 dB, respectively.

ACKNOWLEDGEMENTS

The author is grateful to Professor M. Hamid of the Electrical Engineering Department, University of Manitoba, for suggesting the topic and for his guidance, constant encouragement and constructive criticism throughout this project.

Thanks are also due to Mr. Atef Elsherbeni for his valuable help and profitable discussions, as well as many of my colleagues for their encouragement.

The financial support of the Natural Sciences and Engineering Research Council of Canada and the Department of Electrical Engineering and the Center of Transportation Studies of the University of Manitoba are also gratefully acknowledged

TABLE OF CONTENTS

ABSTRACT iv

ACKNOWLEDGEMENTS v

LIST OF SYMBOLS xi

Chapter page

I. INTRODUCTION 1

II. CORNER ARRAY ANALYSIS AND DESIGN PROCEDURE 7

Schell's Analysis 9
Geometrical Optics Approach 9
Analysis By Neff And Tillman 13
The Production of Low Sidelobe Beams 14
Size of Reflector Surface 15
Extension to Schell's Analysis 16
Directive Gain 16
Design of the Corner Array 17
Equispaced Feed Array 19
Unequispaced Feed Array 20
Results and Discussion 21

III. OFFSET POSITIONING OF ARRAY ELEMENTS 29

Solution of one Offset Feed Element 29
Extension to Multi-element Feed 33
Design Procedure 35
Numerical Results 37

IV. EFFECT OF MUTUAL COUPLING ON THE RADIATION CHARACTERISTICS 43

Introduction 43
Review of Mutual Coupling Theory 47
Current Distribution Along the Feed Dipoles 54
Radiation Pattern 56
Results and Discussion 58

V. EDGE DIFFRACTION EFFECT 70

INTRODUCTION 70
Integral Equation Formulation 72
Solution Of The Integral Equation Formulation . . . 76
Radiation Pattern 77

formulation by the geometrical theory of diffraction 78
Radiation Pattern 80
Computer Programs 82
Results and Discussion 83

VI. CONCLUSIONS 89

Global Optimum 89
Conclusions 90

Appendix page

A. CURRENT DISTRIBUTION ALONG THE FEED DIPOLES 94

B. FAR FIELD RADIATION PATTERN 101

C. FLOW CHART 104

REFERENCES 105

LIST OF TABLES

Table page

2.1. Design Parameters and Radiation Characterstics of Different Corner Arrays (ψ=60°, 3-driven elements) . 26

2.2. Design Parameters And Radiation Characteristics of Different Corner Arrays (ψ=60°, 3-driven elements) . 27

3.1. Parameters and Resulting Radiation Characteristics of the Offset Case (ψ=60°) 40

3.2. Parameters and Resulting Radiation Characteristics of Arbitrary Corner Angle Case (ψ=50° 3-driven elements) 42

4.1. Design Parameter and Radiation Characteristics of Schell Case (ψ=60° 3-driven elements) 62

4.2. Design Parameter and Radiation Characteristics of Case 1 (ψ=60° 3-driven elements) 64

4.3. Design Parameter and Radiation Characteristics of Case 2 (ψ=60° 3-driven elements) 66

4.4. Design Parameter and Radiation Characteristics of highest Gain Case (ψ=60° 3-driven elements) 69

6.1. Design Parameters and Radiation characteristics of Optimum Design (ψ=60°,3-driven elements) 93

LIST OF FIGURES

Figure		page
2.1.	Schematic Diagram of Corner Array	8
2.2.	(a) Waves in a Corner Reflector of Sector angle $\pi/2$ (b) Schematic Representation of the Waves.	10
2.3.	(a) Waves in a Corner Reflector of Sector Angle π/M (b) Schematic Representation of Reflected Waves.	12
2.4.	Radiation Pattern of Case 1 Compared with Schell's Case	24
2.5.	Radiation Pattern of Case 2 Compared with Schell's Case	25
2.6.	Radiation Pattern of Optimum 2	28
3.1.	(a) Offset Fed Corner Reflector (b) Image Diagram for Offset Feed	30
3.2.	Diagram of the Offset Positioning of the Corner Array	34
3.3.	Radiation Pattern of the Offset Case Compared with Schell's Case	39
3.4.	Radiation Pattern of the Arbitrary Corner Angle Case ($\psi=50^\circ$)	41
4.1.	Diagram of the Corner Array	45
4.2.	(a) Image Diagram (b) Ray Diagram from A and B (c) Equivalent Rays when the Ground Plane Removed	46
4.3.	Two Identical Parallel Dipoles	51
4.4.	Radiation Patterns of Schell Case When the Mutual Couplingis Involved	61
4.5.	Radiation Patterns fo Case 1 When the Mutual Coupling is Involved	63
4.6.	Radiation Patterns of Case 2 When the Mutual Coupling is Involved	65

4.7. Radiation Patterns of Case 3 When the Mutual Coupling is Involved 67

4.8. Radiation Pattern corresponding to the higest gain case 68

5.1. Schematic Diagram Of The Corner Array (Finite Wall Length) 71

5.2. Shcematic Diagram of the Closed Surface (two dimension) 73

5.3. Diagram of Images and Edge Images for 60° corner reflector (The space is divided into 22 regions) . . . 79

5.4. Radiation Pattern for Schell case 85

5.5. Radiation Pattern for Equispced Feed Array 86

5.6. Radiation Pattern for Unequispaced Feed Array 87

5.7. Radiation Pattern for the Offset Case 88

LIST OF SYMBOLS

(x,y,z)	-	Cartesian Coordinate System
(r,θ,ϕ)	-	Spherical Coordinate System
(ρ,ϕ,z)	-	Cylindrical Coordinate System
E_z	-	Electric field component in z-direction
E_θ	-	Electric field component in θ-direction
2M-1	-	Number of images
N	-	Number of elements in the feed array
ψ	-	Corner angle
R	-	Main to sidelobe level
$S(\theta,\phi)$	-	Array factor at far field point $P(r,\theta,\phi)$
α,γ	-	Offset angles in azimuth and elevation planes, respectively
$\|I\|$	-	Magnitude of the excitation current
θ	-	Phase of the excitation current
a	-	Dipole wire radius
H	-	Half length of dipole
μ	-	Permeability
η	-	Intrinsic impedance of space
V	-	Driving point voltage
L	-	Reflector length
B.W.	-	Beam width
A_z	-	Z-component of magnetic vector potential
$I_z(Z)$	-	Current distribution along the dipole
$G(\bar{\rho},\bar{\rho}')$	-	Green's function of infinite line source
ω	-	Angular frequency
$J(\bar{\rho}')$	-	Current density on the reflector surface
SLL	-	Sidelobe level

Chapter I

INTRODUCTION

The corner reflector antenna has been extensively used for operation in the VHF and UHF radio frequency ranges. Kraus [1] and Moullin [2] discussed this type of antenna and employed the image theory to calculate the field pattern that applies to the case where the flat walls are of semi-infinite extent. As pointed out by Moullin, the image method appears to be applicable only for flare angles that are submultiples of π . He is rather doubtful as to whether the results expressed as a series of Bessel functions can be generalized to corner reflector apex angles of arbitrary value between 0 and 2π. Wait [3] derived a straightforward solution for the resultant field anywhere within the angle subtended by the corner reflector and he pointed out that Moullin's method of images can easily be extended to arbitrary corner angles . Klopfenstein [4] determined the corner reflector characteristics for reflectors of arbitrary apex angles and excited by any infinitesimal dipole source which is tangent to a circular cylinder having the apex as its axis. He used the dyadic Green's function for the perfectly conducting wedge, and the results obtained involved infinite series of Bessel functions. Neff and Tillman [5] derived a simple expression for the field pattern in terms of infinite series of Bessel functions. Ohba [6] considered reflector antennas finite in wall

length and arbitrary corner angle, using the geometrical theory of diffraction.

Wilson and Cottony [7],[8] gave several experimental radiation patterns for corner reflector antennas having various combinations of width and length of the reflecting surfaces, the corner angle being set at the value that gave a maximum gain for each assembly. Tsai et. al. [9] analyzed the corner reflector both by the moment method and the geometrical theory of diffraction . Redlich [10] gave an approximate solution for the calculation of the radiation pattern of an infinite corner reflector. Kitsuregawa et. al. [11] investigated the offset dipole fed infinite corner reflector antenna. Elsherbeni [12] gave a critical survey of the analysis of corner reflector antennas, and investigated the finite reflector antenna with offset feed using different methods . Elkamchouchi [13] studied the two and the three dimensional cylindrically-capped reflector antennas using image theory.

The corner reflector array was originally introduced by Schell [14], to obtain higher directivity and gain than the conventional corner reflector. The technique used by Schell is to place a linear array of dipoles (or actually monopoles over a ground plane) on the bisector of the corner reflector. Since the positioning of the array elements depends upon the wavelength, the wide bandwidth feature of the corner reflector seems lost. However, if the array elements are considered as the feed and the walls as the reflector, like a parabolic reflector with a horn feed, then the frequency limitations of the antenna are determined by the designer's ingenuity in building and positioning the feed structure.

Schell presented two methods of analysis. The first uses the geometrical optics technique to obtain a solution for the field along the axis of the corner reflector. The second, which is due to Neff and Tillman, is based on images and field from a radiating element on the axis of the reflector . This is extended to yield the field from an array by manipulating the element currents, where it is shown that the sidelobe level within the reflector may be reduced to any desired value. Also, the size of the aperture is shown to correspond to that of other antennas for a given directivity. Finally, the results of the experimental measurements of the properties of two corner arrays are given.

The main objective of this thesis is a much more exhaustive study of the corner array in order to cover the points missed in Schell's design. Specifically, the choice of the feed array positioning for highest gain of an optimum pattern of the antenna can be done more carefully. Also, the effect of offset positioning of the feed elements as well as the mutual coupling and edge diffraction effects need to be considered for a more refined analysis. These four modifications to Schell's design lead to appreciable improvement in the resulting radiation characteristics.

In Chapter II an extension to Schell's analysis for the corner array fed by N infinitesimal dipoles will be introduced. Also, a design procedure for the calculation of the positions is presented on the basis of two related criteria. First, the highest gain corresponding to optimum pattern is denoted by optimum 1 . Second, the maximum gain of the antenna irrespective of the main to side-

lobe level is denoted by optimum 2. The result of an optimization search to calculate the optimum design parameters corresponding to optimum 1 and optimum 2 will be presented. Finally, numerical results for different corner array design and resulting characteristics will be outlined. The radiation characteristics corresponding to each design are tabulated and the corresponding radiation patterns are given.

In Chapter III a more general design of the corner reflector fed by an off-axis array will be introduced. The analysis of this corner array structure will be given in detail using image theory. A specific design procedure of a feed array, symmetrical with respect to the axis of the reflector, will be described. The optimum design parameters and radiation characteristics corresponding to this case are tabulated. The corner array corresponding to an arbitrary corner angle is also investigated in this chapter. An example of a 50° corner angle corresponding to optimum 1, described in Chapter II, is given showing the validity of the analysis and design procedure described in Chapters II and III for arbitrary corner angles.

In Chapter IV the mutual coupling effects on the radiation characteristics are introduced. The method of calculating the mutual coupling is described first for a two dipole array. This method is extended to concentric circular arrays generated from the application of image theory to the corner array. The current distribution along each dipole in the concentric circular array is calculated taking the effect of the mutual coupling into account. This current

distribution is used for the calculation of the radiation pattern and gain of the corner array. The design parameters corresponding to each of the four cases introduced in Chapters II and III are used to re-calculate the radiation characteristics with mutual coupling effects taken into account. The excitation currents corresponding to each case are modified using the Dolph Tchebyscheff technique to generate optimum l again. Another case is introduced for the maximum gain irrespective of the sidelobe level which shows that mutual coupling is important for increasing the gain.

In Chapter V the practical corner array of finite wall length is investigated. The effect of edge diffraction on the radiation pattern is considered. Two methods of solution are introduced. First, the integral equation formulation in which the feed array consists of N line sources positioned anywhere between the finite reflector walls. An integral equation for the current density on the surface of the reflector is derived. The solution of this integral equation is calculated using the moment method. The radiation pattern due to the surface current density and the feed array is evaluated showing the effect of edge diffraction. It should be mentioned here that the gain is calculated in Chapters II, III and IV in three dimensions but in Chapter V the gain is not calculated since the pattern derived is two-dimensional only. Second, the geometric theory of diffraction method used by Ohba [6] is extended to the case of the corner array. In this method the whole space for the example of a 60° corner angle with one feed source is subdivided into 22 regions. This is extended to the multi element

feed case and the pattern is calculated in each region due to N feed dipoles. Numerical results are given at the end of the chapter showing that by increasing the reflector length the sidelobe level and beamwidth decrease. This occurs up to a certain value of the reflector length after which they increase again. The corresponding value of the optimum reflector length is evaluated for each design considered.

Finally numerical results showing how a global optimum, which includes the various factors neglected by Schell, are presented in Chapter VI along with the conclusions.

Chapter II

CORNER ARRAY ANALYSIS AND DESIGN PROCEDURE

The basic structure for the analysis and design of the corner array consists of two perfectly conducting semi-infinite intersecting sheets of corner angle equal to a submultiple of π, fed by an array of N identical infinitesimal dipoles of length 2H (or monopoles of length H over a ground plate) located on the bisector of the corner angle. Fig.2.1 is a schematic diagram of the corner array under consideration and the coordinate system used, where I_i is the amplitude of the driving current of the i<u>th</u> element and ρ_i is the distance from the apex to the i<u>th</u> element. In this case the pattern will be completely derived by the image theory, and the validity of this method for the analysis of the corner reflector antenna is explained by Moullin [2]. In practice, of course, the semi infinite sheets of the ideal model are truncated to some finite extent and, ordinarily, they are made as close to the minimum reflector length as possible. The value of the mathematical model lies in the experimentally observed fact that it predicts the performance of the practical antenna so long as the reflecting sheets are only moderately large relative to the exciting dipoles and the farthest spacing of the array elements from the apex. Schell [14] discussed this arrangement and called it a corner array. The present chapter is an exhaustive treatment of the problem investigated by Schell,

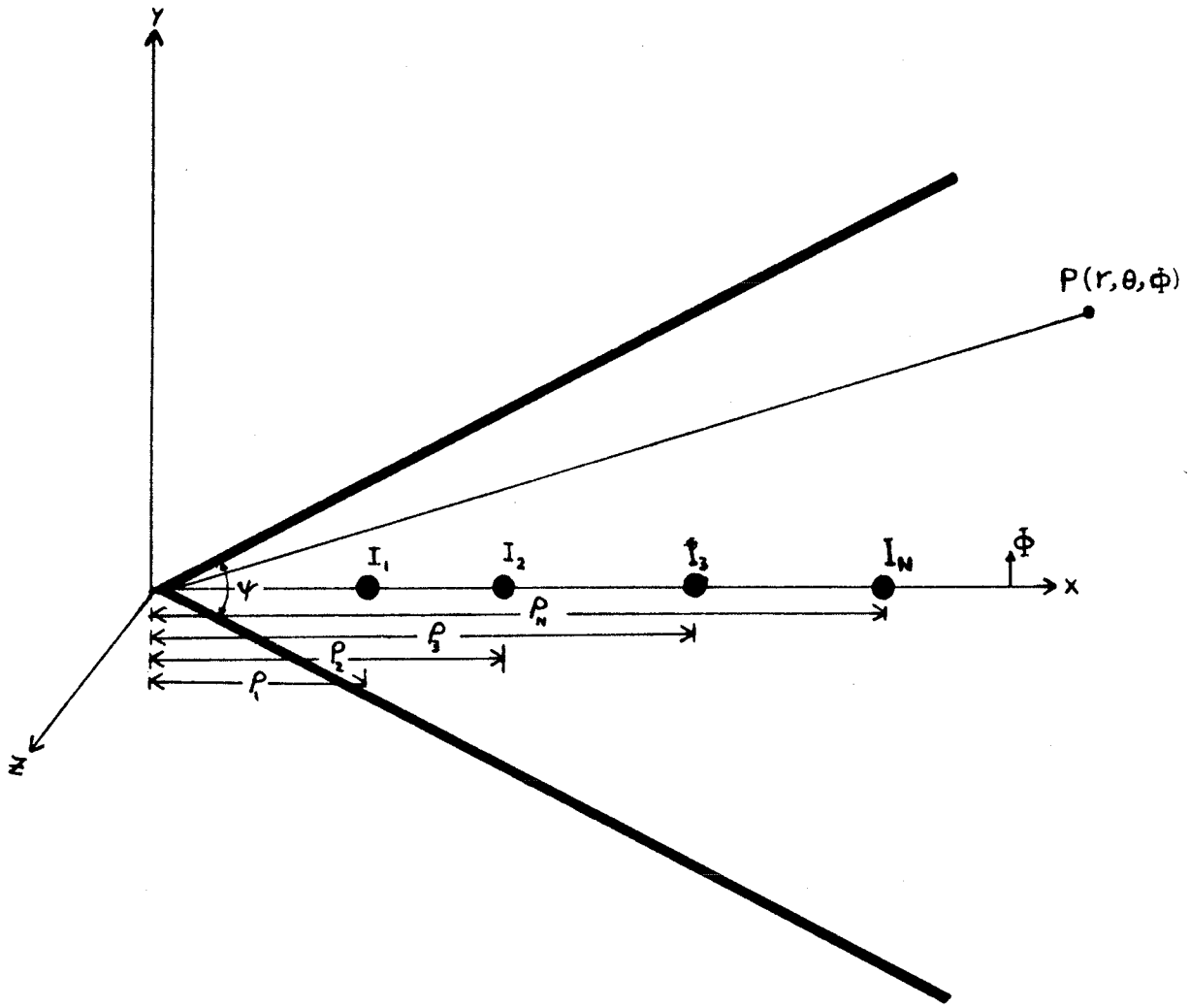

Fig.2.1 : Schematic diagram of corner array.

and a modified design procedure for an optimized system will be given.

2.1 SCHELL'S ANALYSIS

Two methods of analysis are presented. The first uses the geometrical optics technique to obtain a solution for the field along the axis of the corner reflector. The second, which is due to Neff and Tillman, also gives the field from a radiating element on the axis of the reflector. The latter is extended to yield the field from an array.

2.1.1 Geometrical Optics Approach

The field pattern in a corner array is perhaps best determined by first analyzing the simple case of a 90° corner angle and then proceeding to the more general case.

Consider the case of a 90° reflector, consisting of two semi-infinite conducting planes at right angles to one another, as shown in Fig.2.2a. The incident wave suffers two reflections. The resultant waves are shown graphically in Fig.2.2b. Adding these, the total field is found to be

$$E_z = E_o\, e^{-j\beta x} + E_o\, e^{+j\beta x} - E_o\, e^{-j\beta y} - E_o\, e^{+j\beta y} \tag{2.1}$$

$$E_z = 2\, E_o \cos(\beta x) - 2\, E_o \cos(\beta y) \tag{2.2}$$

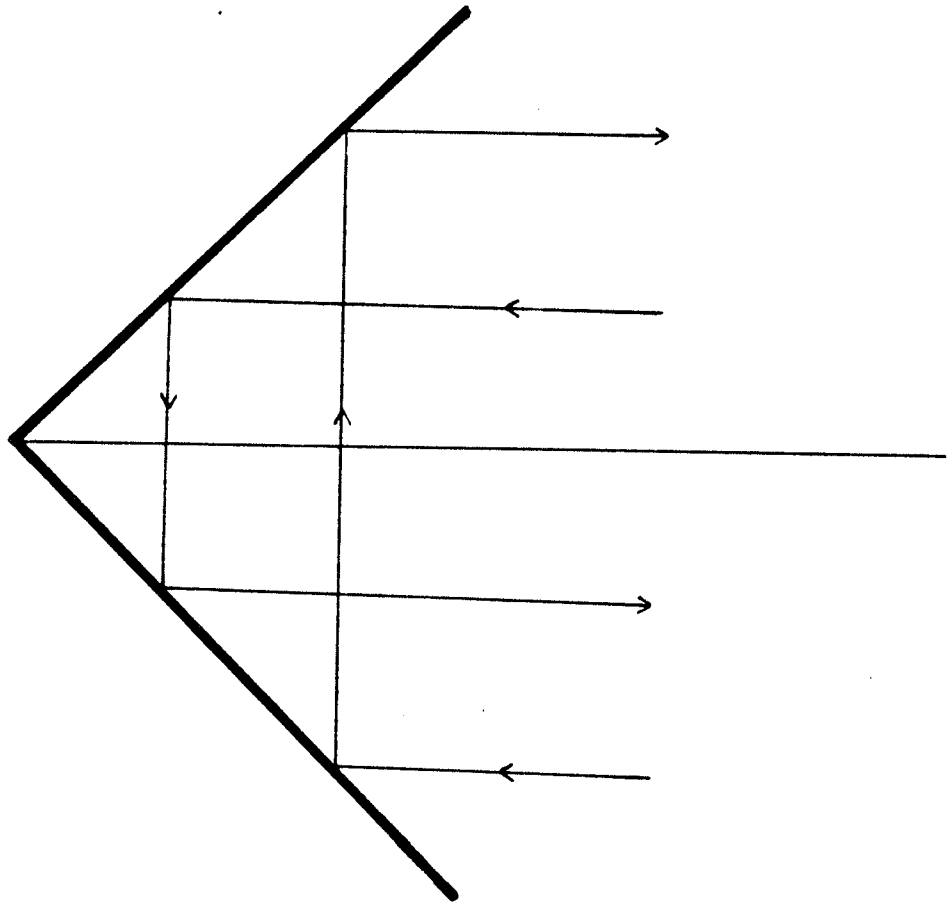

(a)

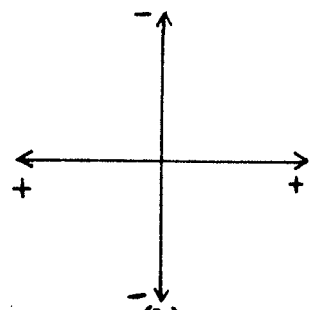

(b)

Fig.2.2 : (a) Waves in a corner reflector of sector angle $\pi/2$.

(b) Schematic representation of reflected waves

With the above example as a guide, it is possible to infer the pattern to be found within two infinite conducting planes intersecting at an angle of π/M radians. This is shown in Fig.2.3 where a (ρ, Φ) coordinate system is used. The result obtained, which is good for $-\pi/2M < \Phi < \pi/2M$, is

$$E_z = (-1)^M \sum_{n=1}^{M} (-1)^n \quad e^{j\beta\rho\cos(\Phi - n\pi/M)} \tag{2.3}$$

It is possible to transform this into a sum of Bessel functions in order to obtain a more useful form of the equation. If this is done, one obtains

for M even,

$$E_z = 4\ M\ E_o \sum_{m=0}^{\infty} J_{(2m+1)M}(\beta\rho) \quad \cos(2m+1)M\Phi \tag{2.4}$$

and for M odd

$$E_z = 4\ j\ M\ E_o \sum_{m=0}^{\infty} (-1)^m\ J_{(2m+1)M}(\beta\rho)\ \cos(2m+1)M\Phi \tag{2.5}$$

A number of dipoles may now be placed at appropriate points ρ_1, $\rho_2, \rho_3 \ldots$ along the bisector of the intersecting planes, and the currents induced in these dipoles (which are proportional to the field strength) may be summed. The total current will then have a variation of the form

$$I_T = I_1 \cos(M\Phi) + I_2 \cos(3M\Phi) + I_3 \cos(5M\Phi) \tag{2.6}$$

for $-\pi/2M < \Phi < \pi/2M$, and will be zero for other values of Φ if the conducting planes appear infinite to the dipoles. However, it may be seen that it is possible to use a number of elements in a corner

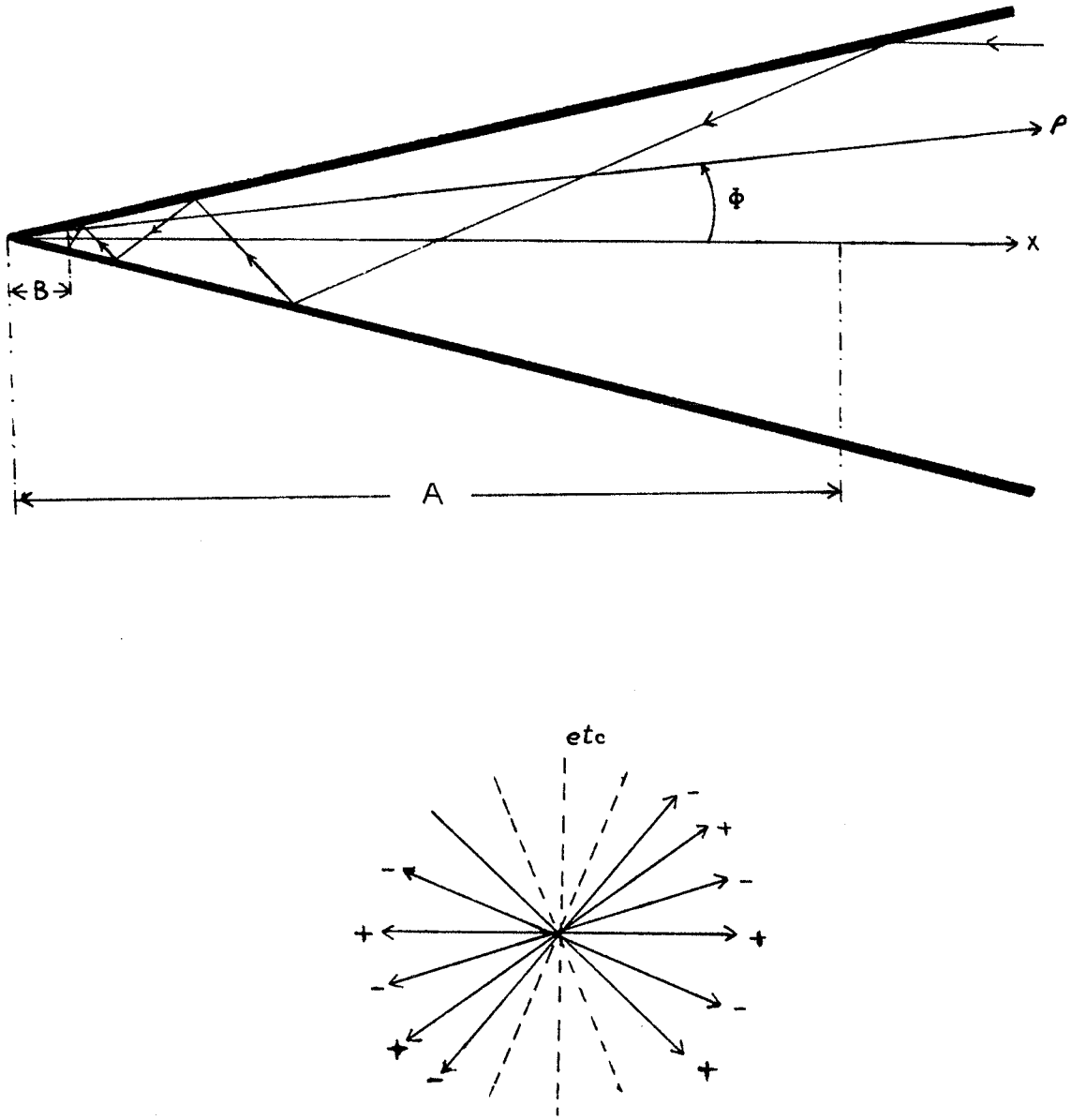

Fig.2.3 (a) Waves in a corner reflector of sector angle π/M .

(b) Schematic represintation of the waves .

reflector, and by appropriately adjusting the currents, to obtain an even radiation pattern within the sector angle of the array. Thus, the inherent directivity and gain of the corner reflector antenna may be enhanced by several times by adding additional elements, provided that the reflector surfaces are sufficiently large.

2.1.2 Analysis By Neff And Tillman

Neff and Tillman have shown a method of analysis of the radiation pattern of the corner reflector antenna for corner angles equal to π/M. They used the method of images and considered the radiation pattern of 2M elements equispaced on a circle of radius ρ. Adjacent images were of opposite polarity provided that the original source element is parallel to the Z axis (i.e. Dirichlett boundary condition). The result obtained is given by

$$E \propto 2\, I_o e^{j\omega t} \left\{ \sum_{n=0}^{\infty} j^{M(2n+1)}\, J_{M(2n+1)}(\beta\rho) \cos M(2n+1)\Phi \right\} \tag{2.7}$$

This approach yields the field from the applied current element, while the previous method of Schell found the standing wave pattern created by an incident wave. Now it is possible to introduce several radiators I_1, I_2, I_3 at radii ρ_1, ρ_2, ρ_3, respectively, to obtain a far field pattern of the form

$$E(\Phi) = A_1 \cos(M\Phi) + A_2 \cos(3M\Phi) + A_3 \cos(5M\Phi) + \cdots\cdots \tag{2.8}$$

In this manner the directivity of the antenna may be increased, provided that the reflector is sufficiently large.

2.1.3 The Production of Low Sidelobe Beams

Obtaining radiation pattern with low main to sidelobe level requires a careful choice of the radiating elements. As an example, consider the design of a 60° corner array with three driven elements and 20 dB main to sidelobe level R within the sector. The element currents are denoted by I_1, I_2 and I_3 and are located at ρ_1, ρ_2 and ρ_3, respectively. Using equation (2.7), the far field pattern is given by

$$\begin{aligned} F(\rho,\Phi) = {} & I_1 [\, J_3(\beta\rho_1)\cos(3\Phi) - J_9(\beta\rho_1)\cos(9\Phi) + J_{15}(\beta\rho_1)\cos(15\Phi) - ..+.] \\ & + I_2 [\, J_3(\beta\rho_2)\cos(3\Phi) - J_9(\beta\rho_2)\cos(9\Phi) + J_{15}(\beta\rho_2)\cos(15\Phi) - ..+.] \\ & + I_3 [\, J_3(\beta\rho_3)\cos(3\Phi) - J_9(\beta\rho_3)\cos(9\Phi) + J_{15}(\beta\rho_3)\cos(15\Phi) - ..+.] \end{aligned} \tag{2.9}$$

One may begin by selecting ρ_1 to correspond to the first maximum of $J_3(\beta\rho_1)$. This makes $J_9(\beta\rho_1)$ and $J_{15}(\beta\rho_1)$ almost zero. Next, one may choose ρ_2 to have such a value that $J_9(\beta\rho_2)$ is near its first maximum and $J_3(\beta\rho_2)$ is nearly zero. If these conditions are met, $J_{15}(\beta\rho_2)$ will also be very small. In choosing ρ_3 it is helpful to pick a point where $J_{15}(\beta\rho_3)$ is near the first maximum and $J_9(\beta\rho_3)$ is nearly zero. The points just described are

$$\beta\rho_1 = 4.0 \qquad \beta\rho_2 = 9.9 \qquad \beta\rho_3 = 17.2$$

The field pattern is then

$$\begin{aligned} F(\Phi) = {} & [\, I_1 J_3(\beta\rho_1) + I_3 J_3(\beta\rho_3)\,]\cos(3\Phi) - I_2 J_9(\beta\rho_2)\cos(9\Phi) \\ & + I_3 J_{15}(\beta\rho_3)\cos(15\Phi) \end{aligned} \tag{2.10}$$

Applying the Dolph Tchebyscheff technique [15] for a 20 dB main to sidelobe level beam in the sector, the following values of the currents are obtained

$$I_1 = 0.775 \quad , \quad I_2 = -1.25 \quad , \quad I_3 = 1.00$$

2.1.4 Size of Reflector Surface

In order to complete the design it is necessary to determine the necessary size of the reflecting surfaces. A quantitatve estimate may be made by applying geometrical optics. Schell found that the location of the source farthest from the apex must not be greater than B, while the reflector length should be greater than A, where

$$B/A = \tan(\pi/2M) \qquad \text{for even } M \tag{2.11}$$

$$B/A = \frac{\tan(\pi/2M)}{\cos(\pi/2M)} \qquad \text{for odd } M \tag{2.12}$$

and the height of the aperture is

$$Y = 2\ A\ \tan(\pi/2M) \tag{2.13}$$

The values obtained from this formulation possess sufficient accuracy for most occasions. However,several parameters have been neglected or not carefully selected in Schell's design. For instance, the choice of ρ_1, ρ_2 and ρ_3 to maximize the gain of the antenna could be done more carefully. Also, the effect of offset positioning of the feed elements as well as the mutual coupling and edge diffraction effects need to be considered for a more refined analysis. These four modifications to Schell's design are the main objectives of this thesis leading to an appreciable improvement in the resulting radiation characteristics.

2.2 EXTENSION TO SCHELL'S ANALYSIS

As an extension to Schell's analysis, the radiation pattern of the corner array illustrated in Fig.2.1 of N feed elements is considered. The feed array consists of N identical infinitesimal dipoles, of length 2H, located on the bisector of the corner angle. The far zone electric field, at $P(r,\theta,\Phi)$, due to one element is given by

$$E_\theta = \frac{2j\omega\mu HI}{4\pi} \frac{e^{-j\beta r}}{r} \sin\theta \tag{2.14}$$

Thus using equation (2.7) derived by Neff and Tillman for a single element feed, one can evaluate the total far zone electric field as

$$E_\theta = \frac{2j\omega\mu H}{4\pi} \frac{e^{-j\beta r}}{r} \sin\theta \; F(\theta,\Phi) \tag{2.15}$$

where

$$F(\theta,\Phi) = 8\,M \sum_{\substack{n=1\\ odd}}^{\infty} (-1)^{nM/2} \left\{ \sum_{i=1}^{N} I_i\, J_{nM}(\beta\rho_i \sin\theta) \right\} \cos(nM\Phi) \tag{2.16}$$

Equation (2.16) gives the far field pattern of this corner array. Also, in order to complete the design requirements, the directive gain can be evaluated as shown next.

2.2.1 Directive Gain

The directive gain can be found in the usual way by comparing the radiation intensity in the preferred direction to the total radiated power. Thus

$$D(\theta_1,\Phi_1) = \frac{4\pi\, I(\theta_1,\Phi_1)}{\int_0^{\Psi}\int_0^{\pi} I(\theta,\Phi)\, \sin\theta\, d\theta\, d\Phi} \tag{2.17}$$

where D is the directive power gain in the direction (θ_1, Φ_1), and I is the radiation intensity in any direction (θ, Φ).

For the corner reflector array excited by infinitesmal dipoles the directive gain can be written as

$$D(\theta_1,\Phi_1) = \frac{4\ \pi\ \sin^2\theta_1 |F(\theta_1,\Phi_1)|^2}{\int_0^{\psi}\int_0^{\pi} |F(\theta,\Phi)|^2 \sin^3\theta\ d\theta\ d\Phi} \tag{2.18}$$

Using equation (2.16) in the denominator, the integration with respect to Φ can be carried out explicitly, and considerable simplification results due to the orthogonality of the trigonometric functions involved in $F(\theta,\Phi)$ on the interval $[-\psi,\psi]$.

Upon integration it is found that

$$D(\theta_1,\Phi_1) = \frac{4\ \pi\ \sin^2\theta_1 |F(\theta_1,\Phi_1)|^2}{\psi \int_0^{\pi/2} \sum_{\substack{n=1\\ odd}}^{\infty} (-1)^{nM} \{ \sum_{i=1}^{\alpha} I_i\ J_{nM}(\beta\rho_i \sin\theta) \}^2\ \sin^3\theta\ d\theta} \tag{2.19}$$

The integration in the denominator of (2.13) can be evaluated numerically.

2.3 DESIGN OF THE CORNER ARRAY

Since our goal is to extend the original design of the corner array, in order to take into account several effects neglected by Schell, it is important to evaluate our extension using the criteria employed by Schell which is effectively the optimum array pattern based on the Dolph Tchebyscheff technique. This optimum will be denoted optimum 1 since there is another optimum, denoted optimum 2, based on the optimum gain of corner array antenna. It

should be emphasized that the Dolph Tchebycheff technique was not derived to take into account the mutual coupling and similar effects. It anticipated that the optimum pattern and optimum gain correspond to different designs.

In the following design procedure, consider a corner array with ψ equal to a submultiple of π, and the reflector surfaces consisting of two semi-infinite intersecting conducting sheets are fed by an array of N infinitesimal dipoles located on the bisector of the corner angle. In this case the radiation pattern at $\theta = \pi/2$ is given by.

$$F(\pi/2,\Phi) = \sum_{\substack{n=1 \\ odd}}^{\infty} (-1)^{nM/2} \left\{ \sum_{i=1}^{N} I_i \; J_{nM}(\beta\rho_i) \right\} \cos(nM\Phi) \tag{2.20}$$

This equation can be written as

$$F(\pi/2,\Phi) = A_1 \cos(M\Phi) + A_2 \cos(3M\Phi) + A_3 \cos(5M\Phi) + \ldots \tag{2.21}$$

where

$$\begin{aligned} A_1 &= (-1)^{M/2} \sum_{i=1}^{N} I_i \quad J_M(\beta\rho_i) \\ A_2 &= (-1)^{3M/2} \sum_{i=1}^{N} I_i \quad J_{3M}(\beta\rho_i) \\ A_N &= (-1)^{(2N-1)M/2} \sum_{i=1}^{N} I_i \quad J_{(2N-1)M}(\beta\rho_i) \end{aligned} \tag{2.22}$$

To start the design procedure, the farthest permissible spacing of the dipoles from the apex should be specified in order to truncate the series (2.21) after a specific number of terms where the higher order Bessel functions approach zero. It is known from [1] that the large spacing from the apex to one feed element gives a pattern with more than one main lobe. Also, numerical computation

shows that as the spacing of the farthest dipoles from the apex is increased further and further the beamwidth starts to increase and accordingly the antenna gain decreases while the pattern will have more than one main beam. For this purpose the maximum permissible spacing in the design procedure is given by the imperical expression

$$\rho_{max} = [\frac{180(2N+1)-3\psi}{2\pi\psi}]\lambda \tag{2.23}$$

This equation was tested for different cases and it gives a good limit (i.e. ρ_{max}) in the design procedure. According to this limiting value, the constant A_{N+1} will be approximately equal to zero and the series (2.21) can be truncated after N terms. The constants A_1 , A_2 , ...and A_N can be evaluated next by the Dolph Tchebyscheff procedure by imposing (2.21) to generate optimum 1 with minimum beamwidth for the specified R. Once the values of the constants A_i are evaluated, the excitation currents I_i can be determined from (2.22) if the element locations ρ_i are specified. In order to determine ρ_i such that the resulting gain is maximum we consider two specific cases of equispaced and unequispaced arrays.

2.3.1 Equispaced Feed Array

When the feed array is equispaced, the location of the first element from the apex ρ_1 and the distance between successive elements d should be specified in order to evaluate the radiation characteristics of the corner array. Since we search for the values of ρ_1 and d of the N elements feed array to generate optimum 1, we have to

take all possible combinations of ρ_1 and d into account. In order to achieve this search, a computer program was designed to evaluate the current in each element using the Dolph Tchebyscheff method for a specific main to sidelobe level R, as well as the radiation pattern and gain for each value of ρ_1 and d. The constraints required for this search are the minimum and maximum values of ρ_1 and d, which are specified in the range of ρ_{max} described above. Also the incremental changes in ρ_1 and d should be supplied to the program. The gain was the objective function in this search. The idea in using equispacing is to reduce the number of parameters in the search procedure from N to two.

2.3.2 Unequispaced Feed Array

The locations of the N elements of the array should be specified for the evaluation of the pattern and gain so that an optimization procedure dealing with N variables inherent in the objective function can be done. A routine ZXMWD from the IMSL library was used for the optimization process. This routine searches for the global minimum or maximum of a function of N variables. An objective function and constraints on the variables under consideration should be supplied externally to this routine. Since in our problem we want to calculate the values of the element locations and excitation currents which generate optimum 1, the gain is taken to be our objective function and the element locations are the variables. The search routine (i.e ZXMWD) specifies values for the variables within the constraints given to it and supplies them to the external

function to calculate the gain. This is repeated so many times until convergence to the local maximum occurs. When the routine supplies the values of the element locations to the external function, the excitation currents are calculated using the Dolph Tchebyscheff technique, which is included in the external function, and the gain is calculated. The optimum values of ρ_i and the corresponding driving currents I_i are listed in the output. The values of ρ_i and I_i are supplied to another program to calculate the radiation pattern and the gain for the corresponding corner array.

2.3.3 Results and Discussion

For the purpose of comparison with Schell's results, an example of 3-driven elements located on the bisector of a 60° corner angle will be investigated throughout. In the first case of an equispaced feed array, a search routine designed to carry out the procedure described above with maximum values for ρ_i and d taken as 2.86λ and 1.3λ, and the minimum values as 0.2λ and 0.25λ, respectively. The best design parameters and resulting radiation characteristics obtained for this case are shown in Table 2.1. Fig.2.3 also shows the radiation pattern of the first case compared with that given by Schell. One can see a decrease of 2.42 dB in the main to sidelobe level R of the first case with respect to Schell's calculations and the beamwidth is slightly decreased. The gain of the first case is higher by 2.02dB than that of Schell. Even in this optimization procedure, where there is a restriction on the element to element separation, the results obtained are much better

than those of Schell indicating that the choice of element locations has significant effect on the performance of this antenna.

In the second case of the unequispaced feed array, the element locations and the driving currents are used to evaluate the radiation pattern and gain of the corner array. The design parameters and resulting radiation characteristics corresponding to this case are shown in Table 2.1. It is apparent that the gain in this case is higher than that of Schell by 2.76 dB while the beamwidth is slightly decreased. Fig.2.4 shows a comparison of the radiation patterns between this case and Schell's case. It is obvious that the main to sidelobe level is lower than that of Schell's case by 2.61 dB and the position of the first null is the same as that of Schell. It should be noted from this case that the farthest element from the apex is at a distance of 2.433 λ which is lower than Schell's design by 0.307 λ. This reduction makes the antenna size smaller than that of Schell. As can be seen from the results of this case, there are many advantages over Schell's design and they are basically due to the correct manipulation of the element locations which are the most important parameter in this design procedure.

For the evaluation of optimum 2 described before, one can follow the optimization procedure described for unequispaced feed array. This optimization procedure is repeated for different values of main to sidelobe level. The results obtained show that the gain increases with the increase of main to sidelobe level up to a certain level then decreases with further increase in the main to si-

delobe level. Table 2.2 shows the results obtained corresponding to this behaviour. It is seen from this table that the maximum value of the gain is 19.958 dB and the corresponding main to sidelobe level and beamwidth are 16.96dB and 9.73°, respectively. The radiation pattern corresponding to this optimum 2 is shown in Fig.2.6.

In this chapter, the generalized analysis and design procedure are introduced to calculate the design parameters and radiation characteristics of the corner array. Two factors are ignored in the above analysis. These are the effect of mutual coupling between elements and the effect of edge diffraction on the radiation characteristics. These factors will be investigated in the next chapters and the modified design leading to improvements in the radiation characteristics will be presented.

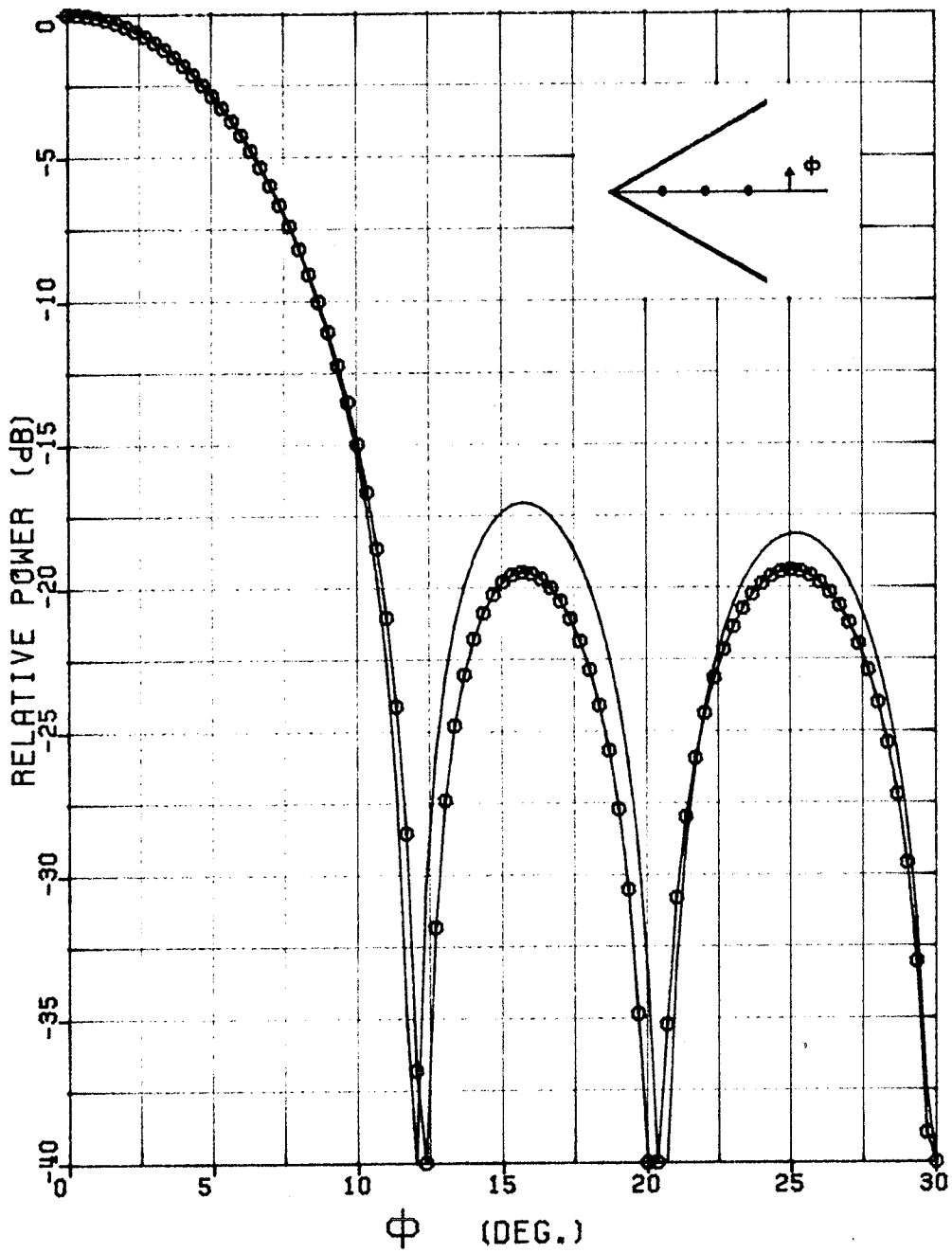

FIG.2.4: RADIATION PATTERN FOR

— SCHELL

⊖⊖⊖ CASE 1

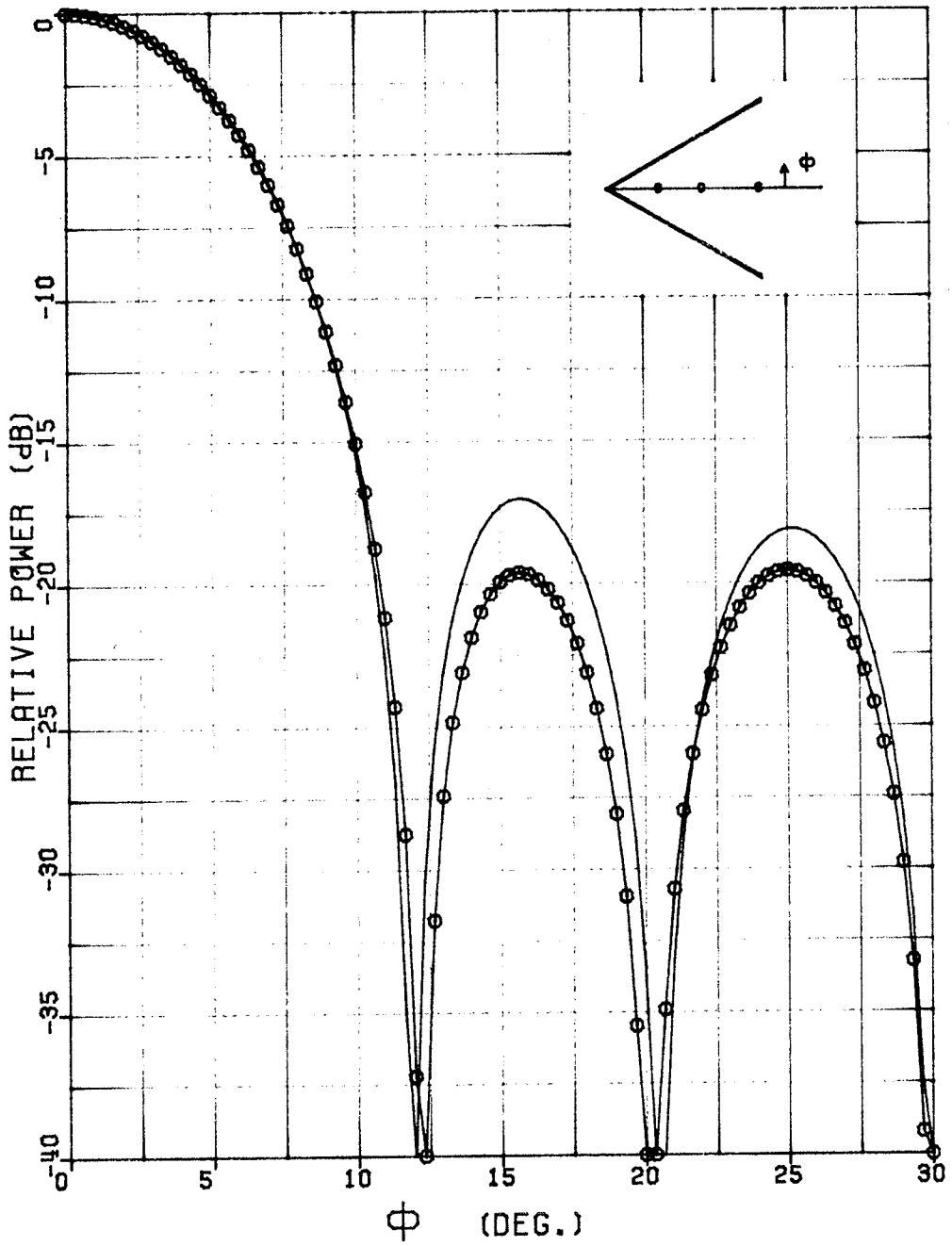

FIG.2.5: RADIATION PATTERN FOR

— SCHELL

-888- CASE 2

TABLE 2.1

Design Parameters and Radiation Characterstics of Different Corner Arrays (ψ =60°, 3-driven elements)

	Schell	Case 1	Case 2
I_1	0.775	1.000	1.000
I_2	-1.250	-0.130	-0.336
I_3	1.000	0.180	0.300
ρ_1/λ	0.640	0.240	0.300
ρ_2/λ	1.580	1.380	1.100
ρ_3/λ	2.740	2.520	2.433
Gain (dB)	16.92	18.94	19.679
R (dB)	17.02	19.44	19.61
B.W. (Deg.)	10.31	10.23	10.19

TABLE 2.2

Design Parameters And Radiation Characteristics of Different Corner Arrays (ψ=60°, 3-driven elements)

R (dB)	B.w. (Deg.)	ρ_1/λ	ρ_2/λ	ρ_3/λ	I_1	I_2	I_3	Gain (dB)
13.7	9.2	0.323	0.950	2.524	1.00	-0.196	0.337	19.581
15.24	9.5	0.313	0.950	2.489	1.00	-0.192	0.255	19.857
15.6	9.53	0.300	0.950	2.480	1.00	-0.171	0.221	19.894
16.26	9.63	0.300	0.950	2.464	1.00	-0.180	0.206	19.944
16.58	9.68	0.300	0.950	2.456	1.00	-0.183	0.199	19.954
16.96	9.73	0.300	0.950	2.448	1.00	-0.187	0.193	19.958
17.19	9.78	0.302	0.950	2.440	1.00	-0.194	0.192	19.948
17.75	9.86	0.300	0.950	2.423	1.00	-0.196	0.180	19.907
18.73	10.04	0.300	1.051	2.430	1.00	-0.269	0.253	19.788
19.61	10.19	0.300	1.100	2.433	1.00	-0.336	0.300	19.679
20.4	10.44	0.300	1.132	2.436	1.00	-0.400	0.339	19.587
21.13	10.44	0.300	1.152	2.437	1.00	-0.463	0.366	19.499
21.79	10.55	0.305	1.163	2.437	1.00	-0.547	0.404	19.418
22.41	10.66	0.305	1.179	2.440	1.00	-0.607	0.429	19.345

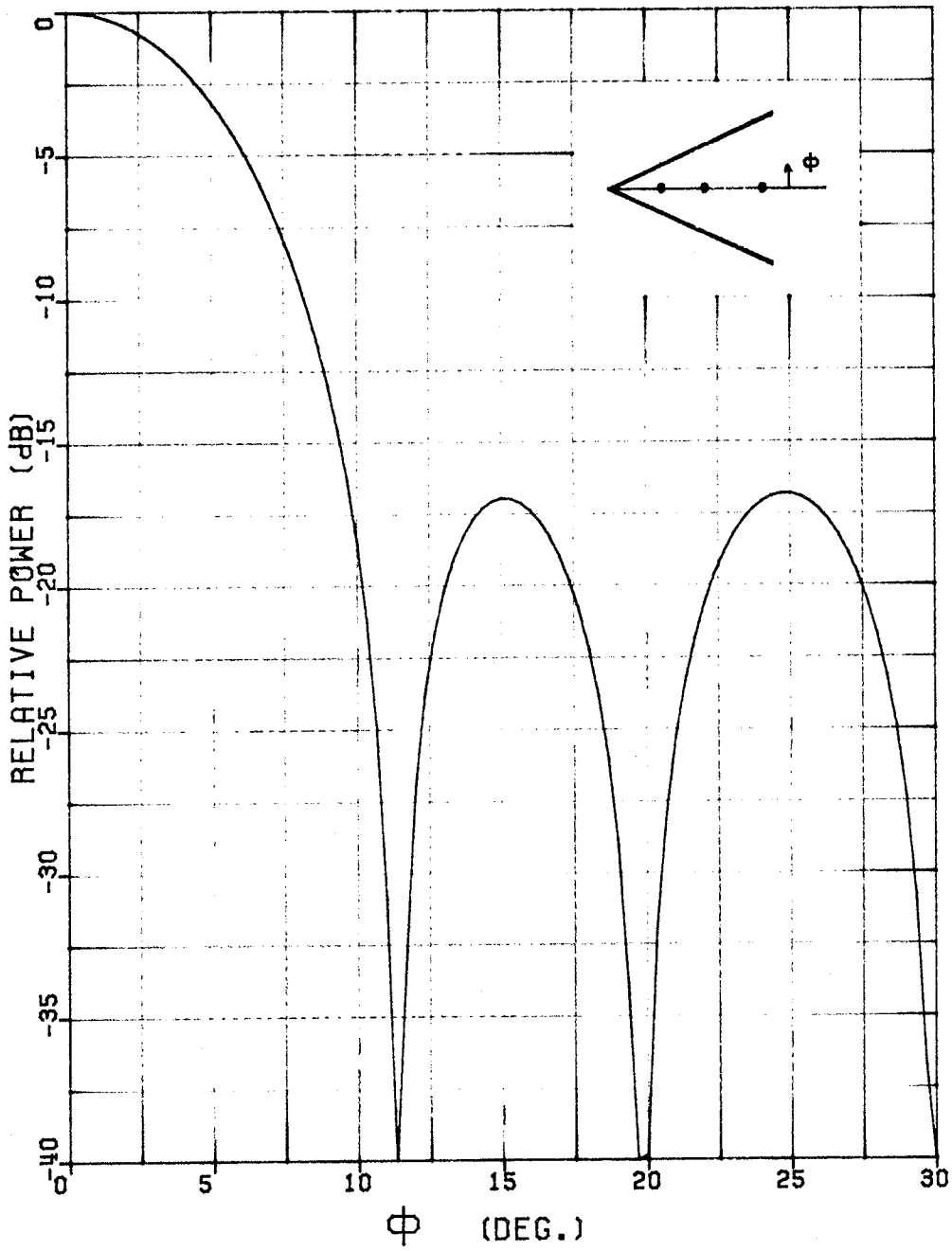

FIG.2.6: RADIATIØN PATTERN FØR ØPTIMUM 2

Chapter III

OFFSET POSITIONING OF ARRAY ELEMENTS

A more general design of the corner array can be achieved by manipulating the positions of the feed array elements off the axis of the reflector. The proper choice of position and excitation currents of the elements may yield higher gain for optimum array pattern. In the following analysis and proposed design of the corner array, the reflector angle ψ is taken as a submultiple of π and image theory is applied in the same manner as for semi-infinite walls.

3.1 SOLUTION OF ONE OFFSET FEED ELEMENT

Consider the corner reflector shown in Fig.3.1a where ρ is the distance between the apex and the current element I and α is the offset angle. Since ψ is a submultiple of π, the application of image theory gives a circular array as shown in Fig.2.1b. The reversal of current direction upon each reflection is displayed by $\otimes$ and $\odot$ for currents into and out of the plane of the paper, respectively.

The number of images including the original source is 2M, where

$$M = \pi/\psi \quad , \quad M \text{ integer} \tag{3.1}$$

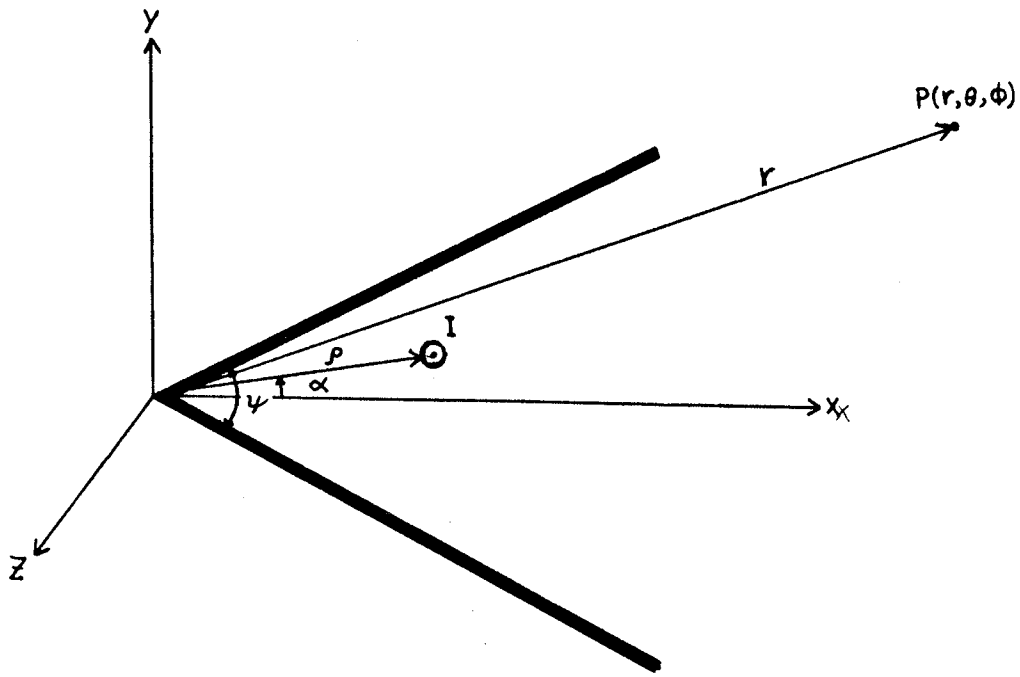

(a)

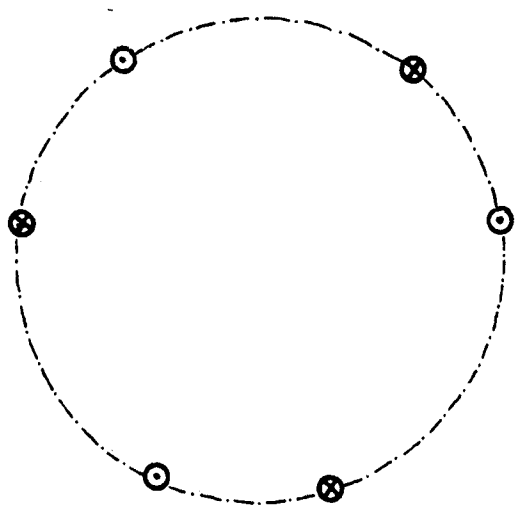

(b)

Fig.3.1 : (a) Offset fed corner reflector .

(b) Image diagram for offset feed .

The polar angle Φ_i of the i<u>th</u> element in the circular array is given by

$$\Phi_i = (i-1)\ \psi + (-1)^{i-1}\ \alpha \tag{3.2}$$

The array factor at a far point $P(r,\theta,\Phi)$ is given by

$$S(\theta,\Phi) = I \sum_{i=1}^{2M} (-1)^{i-1} \quad e^{j\,z\cos\eta_i} \tag{3.3}$$

where

$$\eta_i = \Phi - \Phi_i$$
$$z = \beta\ \rho\ \sin\theta \tag{3.4}$$

Equation (3.3) may be expanded in a series of Bessel fuctions [16], giving

$$S(\theta,\Phi) = I \sum_{i=1}^{2M} (-1)^{i-1} \ \{\ J_o(z) + 2 \sum_{k=1}^{\infty} (-1)^k \ J_{2k}(z) \ \cos(2k\eta_i)$$
$$+2j \sum_{k=0}^{\infty} (-1)^k \ J_{2k+1}(z) \ \cos(2k+1)\eta_i\} \tag{3.5}$$

each term of equation (3.5) may be considered separately. Let

$$S_1 = \sum_{i=1}^{2M} (-1)^{i-1} \ J_o(z) \tag{3.6}$$

$$S_2 = 2 \sum_{i=1}^{2M} (-1)^{i-1} \sum_{k=1}^{\infty} (-1)^k \ J_{2k}(z) \ \cos(2k\eta_i) \tag{3.7}$$

$$S_3 = 2j \sum_{i=1}^{2M} (-1)^{i-1} \sum_{k=o}^{\infty} (-1)^k \ J_{2k+1}(z) \ \cos((2k+1)\eta_i) \tag{3.8}$$

Now in each case these sums are reduced to geometric progressions. The first is

$$S_1 = \sum_{i=1}^{2M} (-1)^{i-1} \; J_o(z) \tag{3.9}$$

Since 2M is an even number, it can be shown that

$S_1 = 0.0$

By reversing the order of summation and by using a simple algebraic manipulation, one obtains for S_2

$$S_2 = \sum_{k=1}^{\infty} (-1)^k \; J_{2k}(z) \sum_{i=1}^{2M} (-1)^{i-1} \{ \; e^{j2k(\Phi-\Phi_i)} + e^{-j2k(\Phi-\Phi_i)} \; \} \tag{3.10}$$

S_2 may now be simplified by summing the geometric progression, i.e.

$$S_2 = 2 \sum_{k=1}^{\infty} (-1)^k \; J_{2k}(z) \; \{\cos k(2\Phi-2\alpha-(2N-2)\psi) - \cos(2\Phi+2\alpha-2M\psi)\} \; \sin(2kN\psi)/\sin(2k\psi) \tag{3.11}$$

In equation (3.11), M and k are integers and the only values of k which give rise to nonzero terms are those for which

$$k = n\pi/2\psi \quad , \quad n=1,2,.... \tag{3.12}$$

Using (3.12) in equation (3.11) leads to

$$S_2 = 4M \sum_{n=1}^{\infty} (-1)^{n\pi/2\psi} \; J_{n\pi/\psi}(\beta\rho\sin\theta) \; \sin n\pi(\Phi/\psi + 1/2) \; \sin n\pi(\alpha/\psi + 1/2) \tag{3.13}$$

The summation S_3 can be carried out by the same way as for S_2. Hence the result obtained by adding S_1, S_2 an S_3 is given by

$$S(\theta,\Phi) = (8I\pi/\psi) \sum_{n=1}^{\infty} (-1)^{n\pi/2\psi} \; J_{n\pi/\psi}(\beta\rho\sin\theta) \; \sin n\pi(\Phi/\psi + 1/2) \; \sin n\pi(\alpha/\psi + 1/2) \tag{3.14}$$

Equation (3.14) gives the pattern for one offset feed element in a corner reflector antenna within the corner angle. It should be mentioned here that, although equation (3.14) is derived from the image theory for corner angles equal to submultiples of π, it can be used for any arbitrary corner angle [4]. The only analytical difficulty in generalizing equation (3.14) is that S is not equal to zero when Φ equals $2\pi+\psi/2$ unless ψ is a submultiple of π. However since Φ is restricted to the range $-\psi/2 < \Phi < \psi/2$ due to the semi-infinite walls, equation (3.14) is valid and general for arbitrary corner angles.

3.2 EXTENSION TO MULTI-ELEMENT FEED

The corner array geometry under consideration is shown in Fig.3.2. The feed array consists of N identical infinitesimal dipoles located anywhere between the semi-infinite reflecting walls. Due to the principle of superposition, the array factor of equation (3.14) can be extended to the case of N element feed giving

$$S(\theta,\Phi) = (8\pi/\psi) \sum_{n=1}^{\infty} (-1)^{n\pi/2\psi} \left\{ \sum_{i=1}^{N} I_i \; J_{n\pi/\psi}(\beta\rho_i \sin\theta) \; \sin n\pi(\alpha_i/\psi + 1/2) \right\} \sin n\pi(\Phi/\psi + 1/2) \tag{3.15}$$

where ρ_i is the radial distance between the apex and the i<u>th</u> dipole and α_i is the offset angle of the i<u>th</u> dipole. The far zone electric field at $P(r,\theta,\Phi)$ of an infinitesimal dipole is given by

$$E_\theta = \frac{2j\omega\mu HI}{4\pi} \frac{e^{-j\beta r}}{r} \sin\theta \tag{3.16}$$

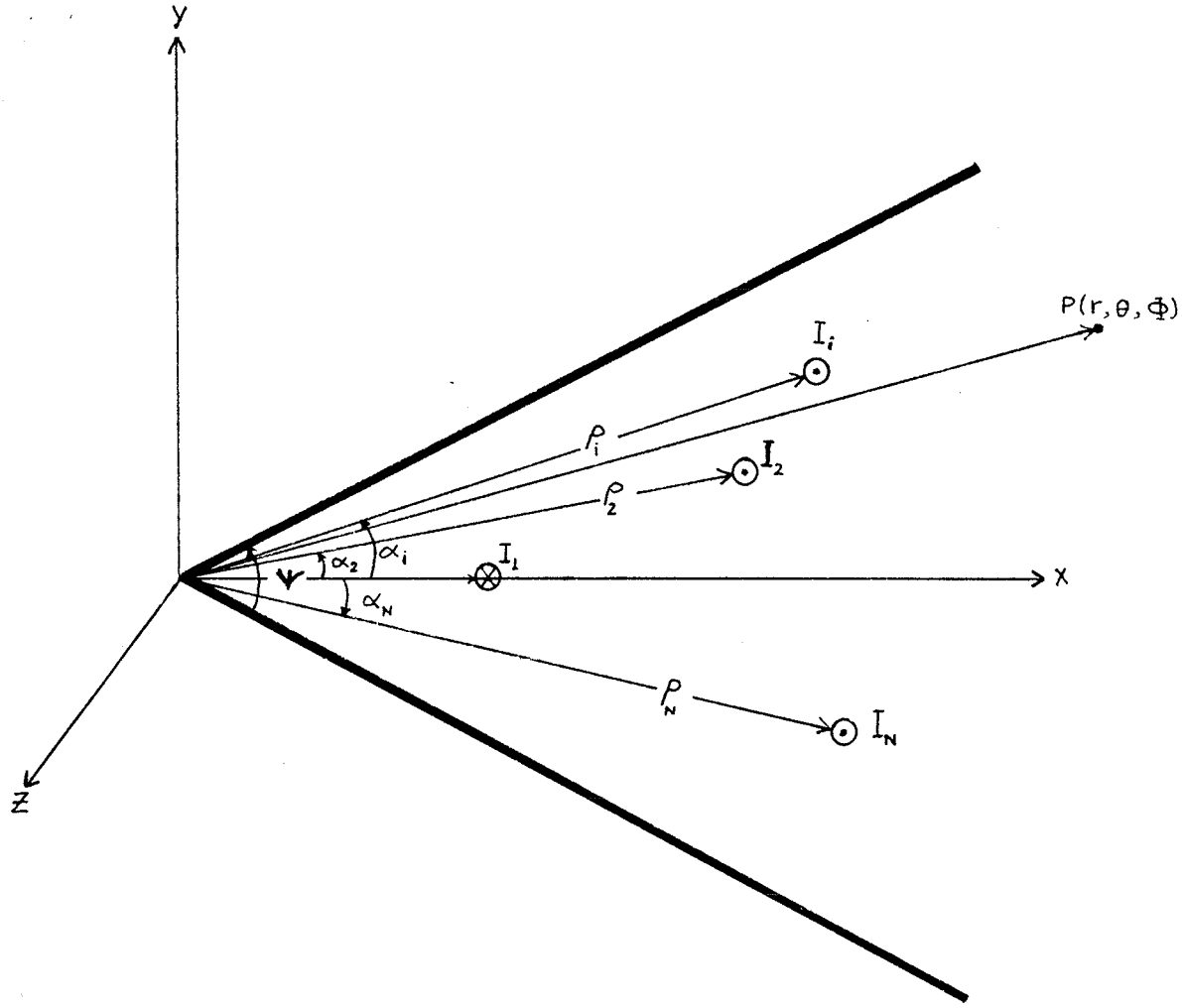

Fig.3.2: Diagram of the offset positioning of the corner array .

where μ is the permeability of the air and 2H is the dipole length. In this case the total far zone electric field from the corner array is given by

$$E_\theta = \frac{2j\omega\mu H}{4\pi} \frac{e^{-j\beta r}}{r} \sin\theta \; S(\theta,\Phi) \tag{3.17}$$

The infinite series in equation (3.15) is rapidly convergent when the farthest element spacing from the apex is kept smaller than ρ_{max} given by (2.19) .

3.3 DESIGN PROCEDURE

The main purpose in the following design procedure is getting highest gain for optimum pattern. If the maximum element spacing from the apex is given by equation (2.19), then the infinite series (3.15) can be truncated after (2N-1) terms, where N is the number of the feed elements. The evaluation of a low main to sidelobe level pattern using the Dolph Tchebyscheff technique can be achieved by considering a symmetrical feed array around the axis of the reflector. To clarify this, consider a corner array of 60° corner angle fed by 3-driven elements. The feed array is arranged such that it is symmetrical with respect to the axis of the reflector. In doing so, one can choose the offset angles as 0°, 15° and -15° and the distances from the apex as ρ_1 , ρ and ρ as shown in Fig. 3.3. Also the corresponding excitation currents are labelled as I_1 , I and I. In this case one can write

$$\begin{aligned} |S(\pi/2,\Phi)| = &\{ I_1 \, J_3(\beta\rho_1) + \sqrt{2}\, I \, J_3(\beta\rho)\} \cos(3\Phi) \\ &+\{I_1 \, J_9(\beta\rho_1) - \sqrt{2}\, I \, J_9(\beta\rho)\} \cos(9\Phi) \\ &+\{ I_1 \, J_{15}(\beta\rho_1) - \sqrt{2}\, I \, J_{15}(\beta\rho)\} \cos(15\Phi) \end{aligned} \tag{3.18}$$

Equation (3.18) can be written as

$$|S(\pi/2,\Phi)| = A_1 \cos(\Phi') + A_2 \cos(3\Phi') + A_3 \cos(5\Phi') \tag{3.19}$$

where

$\Phi' = 3\Phi$

$$\begin{aligned} A_1 &= I_1 J_3(\beta\rho_1) + \sqrt{2}\, I\, J_3(\beta\rho) \\ A_2 &= I_1 J_9(\beta\rho_1) - \sqrt{2}\, I\, J_9(\beta\rho) \\ A_3 &= I_1 J_{15}(\beta\rho_1) - \sqrt{2}\, I\, J_{15}(\beta\rho) \end{aligned} \tag{3.20}$$

The Dolph Tchebyscheff conditions for a 20 dB main to sidelobe level can be applied to equation (3.19) giving the corresponding values of the A's as

$$A_1 = 1.85 \qquad A_2 = 1.437 \qquad A_3 = 1.00 \tag{3.21}$$

Once the values of the coefficients are evaluated, the excitation currents I_1 and I can be evaluated from (3.20) if the values of ρ_1 and ρ are specified. In this case an optimization search should lead to the values of ρ_1 and ρ at which the maximum gain occurs. The search technique is based on specifying the values of ρ_1 and ρ and calculating the corresponding excitation currents as well as the gain. By taking all possible combinations of ρ_1 and ρ between 0 and ρ_{max}, and computing the gain in each iteration, the values of ρ_1 and ρ corresponding to the highest gain are selected.

3.4 NUMERICAL RESULTS

A search routine was prepared to carry out the above design procedure. The best locations and excitation currents obtained from the search are shown in Table 3.1. Also the radiation characteristics corresponding to these design parameters are evaluated. As can be seen, the gain is increased by 2.12 dB over that of Schell. For the radiation pattern in Fig.3.3, one can see a decrease of 1.31 dB in the main to sidelobe level and 0.62° in the beamwidth over the corresponding results of Schell. The results obtained in this case are not the universal optimum, but they are the optimum within the constraints already specified. For the case of an arbitrary corner angle, the specific value of ψ equal to 50° was investigated througth out. The case of an unequispaced feed array along the bisector for a 50° corner angle is also investigated numerically. The design procedure explained in chapter II is applied giving the design parameters and the radiation characteristics shown in Table 3.2, where $|I_i|$ and θ_i denote the magnitude and phase of the excitation current in element i, respectively. The results obtained for this case indicate that the gain is 19.84 dB while, from Fig.2.4 for the radiation pattern, the main to sidelobe level is 20.13 dB and the beamwidth is 8.38° which are better than all other cases of 60° corner arrays given in chapter II. The farthest element from the apex in the feed array is located at 3.1λ. This is a relatively large distance and makes the antenna size larger than the 60° corner arrays also given in chapter II. The 50° corner angle shows that the above analysis and design procedure can be gen-

eralized for arbitrary corner angles and illustrates one of the parameters not specifically emphasized by Schell.

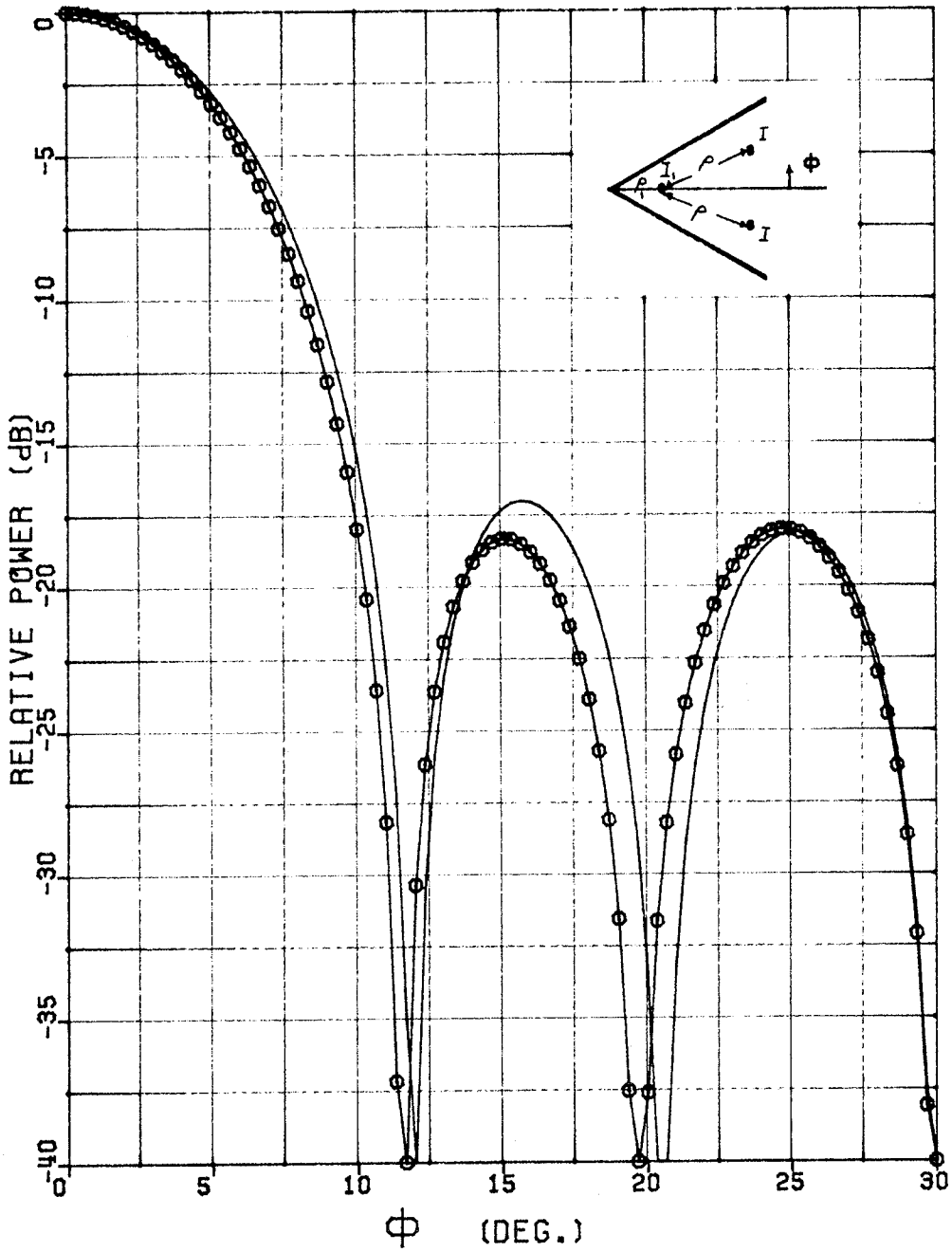

FIG.3.3: RADIATION PATTERN FOR

— SCHELL

OFFSET

TABLE 3.1

Parameters and Resulting Radiation Characteristics of the Offset Case (ψ=60°)

	Element (1)	Element (2)	Element (3)
I	1.00	-0.60	1.00
ρ/λ	2.35	0.315	2.35
α	-15.0	0.00	15.0
Gain (dB)	19.04		
R (dB)	18.33		
B.W. (Deg.)	9.69		

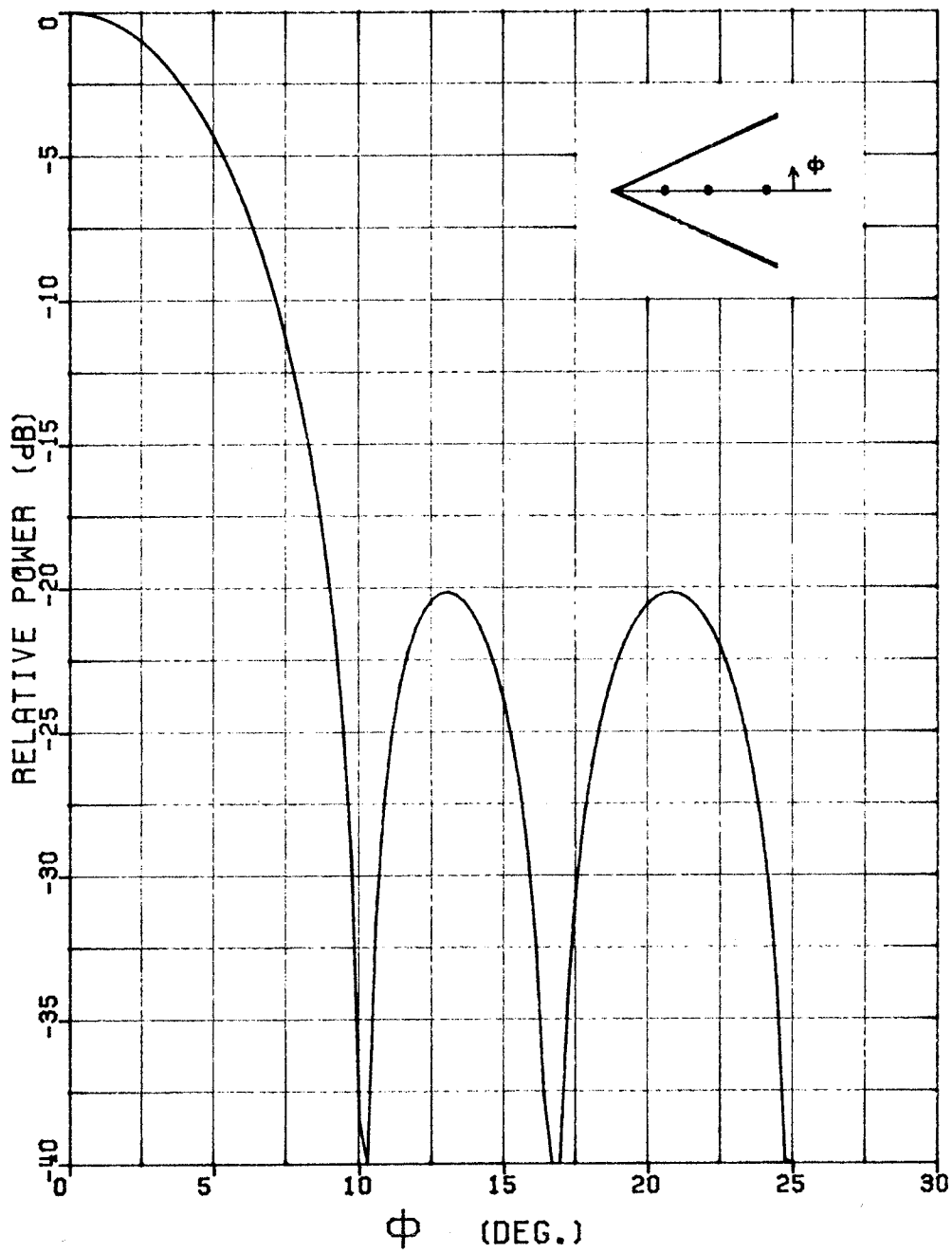

FIG.3.4: RADIATION PATTERN FOR 50° CORNER ARRAY

TABLE 3.2

Parameters and Resulting Radiation Characteristics of Arbitrary Corner Angle Case (ψ=50° 3-driven elements)

	Element (1)	Element (2)	Element (3)
$\|I\|$	1.000	0.914	0.775
θ	178.6	92.7	-179.4
ρ/λ	1.30	1.90	3.10
Gain (dB)	19.844		
R (dB)	20.12		
B.W. (Deg.)	8.39		

Chapter IV

EFFECT OF MUTUAL COUPLING ON THE RADIATION CHARACTERISTICS

4.1 INTRODUCTION

In practice, the feed array consists of a number of cylindrical dipoles arranged between the reflector walls such that the current distribution along each dipole is modified by mutual coupling effects in the composite structure. In this chapter the effect of mutual coupling between the feed dipoles themselves and between them and the reflector surface is considered.

The earliest treatments of the cylindrical center-driven dipole antenna as a boundary value problem are those of King [18] and Hallen [19] who used essentially the retarded potential method of Pocklington [20]. Hallen derived an integral equation for the current distribution along the dipole and solved the resulting integral equation by a method of iteration in reciprocal powers of a parameter which is equal to 2 ln 2H/a, where H is the half length of the dipole and 'a' is the radius. Schelkunoff [21] presented a different treatment based on the non-uniform transmission line method. His starting point was the thin biconical antenna, which he solved as a boundary value problem concentrating on the fields rather than the current distributions. To apply the biconical antenna solution to the cylindrical case, Schelkunoff used a

perturbation method. The conical boundary was considered perturbed into the cylindrical shape and the perturbed wave functions calculated. King et. al. [22] used a different expansion parameter in the iteration of Hallen's integral equation in order to achieve more rapid convergence. This is the so called King-Middleton expansion. The method of analysis used here for the evaluation of the mutual coupling was proposed by King et. al. [17], who used an approximate method for solving an appropriate integral equation to evaluate the current distribution along each dipole.

Consider the corner array shown in Fig.(4.1), where the corner angle is a submultiple of π. In this case, image theory can be applied giving a concentric circular array as shown in Fig.(4.2a), with each circular array containing 2M elements including the source. The images around the circumference of each circular array are symmetrically positioned with respect to each other and to the elements of the other circular arrays.

Before determination of the mutual coupling, the physical interpretation of the mutual coupling is considered. Since the imaging process of the corner array is simply multiple imaging on an infinite perfectly conducting sheet , a simple example of two dipoles above an infinite ground plane is considered. Fig.(4.2b) is a diagram of the rays incident from two sources, A and B, and the reflected rays from the ground plane. Fig.(4.2c) gives the equivalent rays when the ground plane is removed and the images of A and B are presented. From these ray diagrams we conclude that there is a mutual coupling between

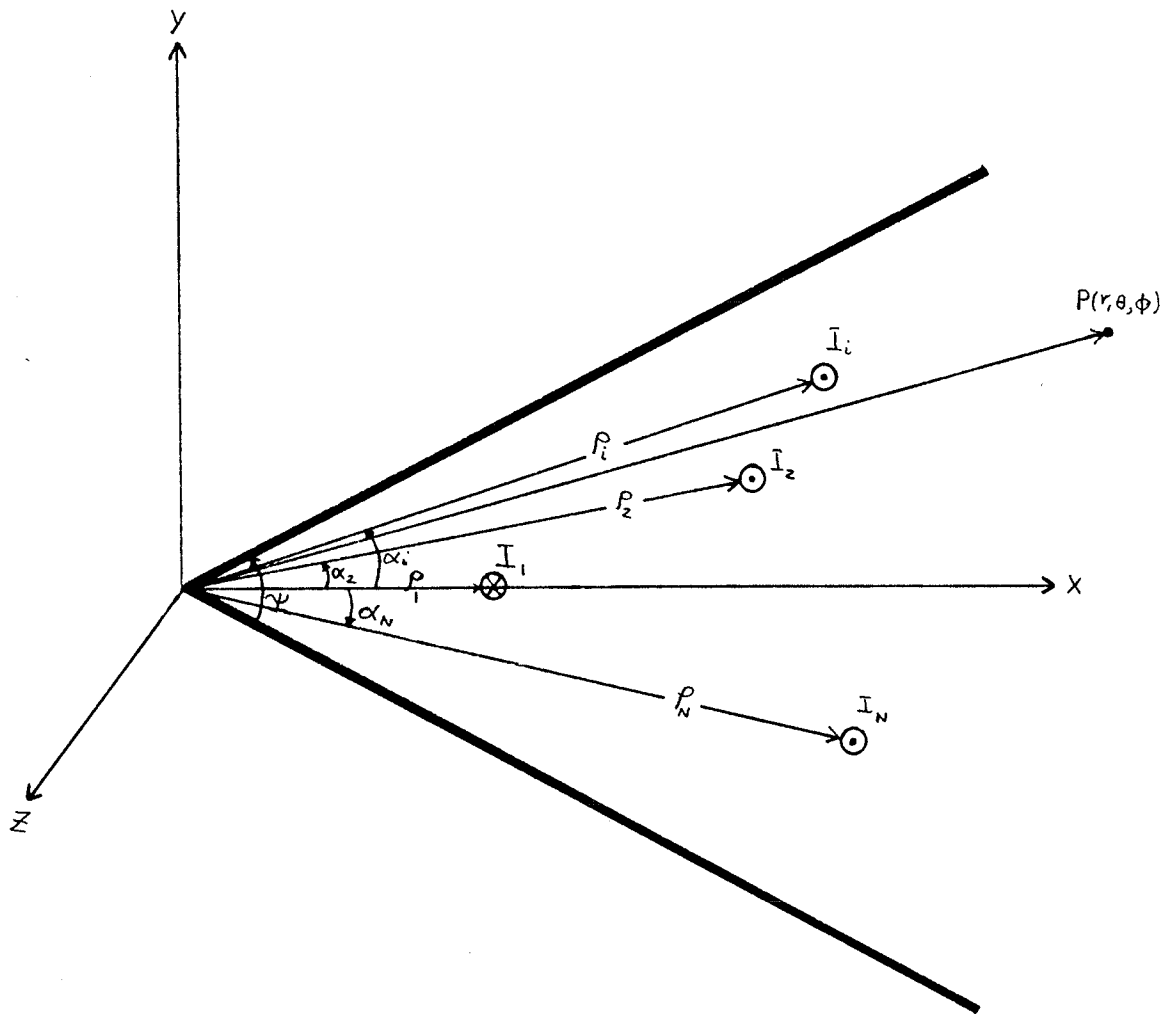

Fig.4.1 : Diagram of the corner array .

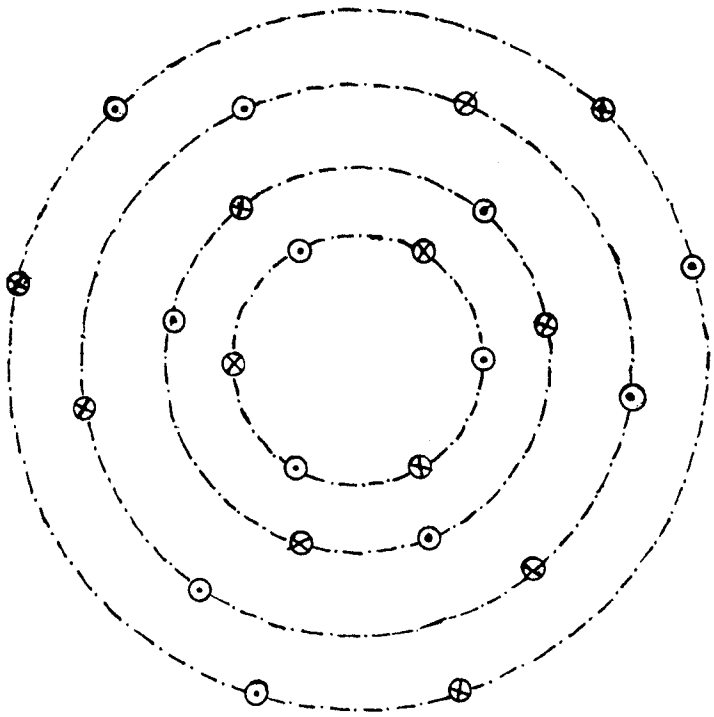

(a)

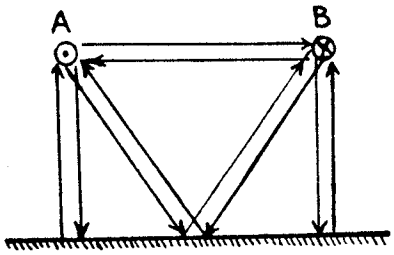

(b)

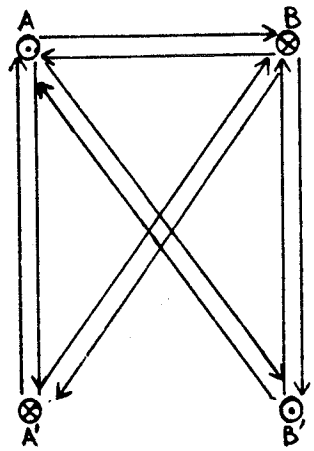

(c)

Fig.4.2 : (a) Image digram .
(b) Ray digram from A and B .
(c) Equivalent rays when the ground plate removed.

1. any source and all other sources
2. each source and its own images
3. each source and all images of the other sources

According to the above model, the current distribution along each feed dipole is evaluated considering the various mutual coupling terms.

4.2 REVIEW OF MUTUAL COUPLING THEORY

To illustrate the method of calculating the effect of mutual coupling, an example of a two element array is considered. Since the individual elements in the array may be quite close to each other, the excitation currents in them will necessarily interact. It follows that the amplitude and phase distribution of the current along each element depends not only on the length, radius, and driving voltage of that element, but also on the distribution in the amplitude and phase of the currents along all elements in the array. Assuming that the elements of the array are located along the Z-axis, the integral equation for the magnetic vector potential for a conducting cylindrical dipole of length 2H and radius 'a' with its center at Z = 0 is given by [17]

$$A_z = (\mu/4\pi) \int_{-H}^{H} I_z(z') \, (e^{-j\beta R1}/R1) \, dz' \tag{4.1}$$

where

$$R1 = \sqrt{(z-z')^2 + a^2} \tag{4.2}$$

Also, from the boundary condition $E_z(z) = 0$ on the surface $\rho = a$ of a perfectly conducting dipole, the vector potential is seen to satisfy the equation

$$(d^2/dz^2+\beta^2)\ A_z(z)=0 \tag{4.3}$$

which has the solution

$$A_z(z) = (-4j\pi/\eta)\ (C_1 \cos(\beta z) + C_2 \sin(\beta|z|)) \tag{4.4}$$

where C_1 and C_2 are arbitrary constants of integration. If the symmetry conditions

$$I_z(-z) = I_z(z) \qquad ,A_z(-z) = A_z(z) \tag{4.5}$$

are imposed, then the value of C_2 can be obtained as

$$C_2 = (1/2)\ V_o \tag{4.6}$$

From (4.1), (4.4) and (4.6) one can obtain

$$\begin{aligned} 4\pi\mu^{-1}\ A_z(z) &= {}_{-H}\int^{H} I_z(z')\ (e^{-j\beta R1}/R1)\ dz' \\ &= (-4j\pi/\eta)\ (C_1 \cos(\beta z) + (1/2)V_o \sin(\beta|z|)) \end{aligned} \tag{4.7}$$

Subtracting $4\pi\mu^{-1}A_z(H)$ from both sides of equation (4.7) one gets

$$\begin{aligned} 4\pi\mu^{-1}[A_z(z)-A_z(H)] &= {}_{-H}\int^{H} I_z(z')\ K_d(z,z')\ \ dz' \\ &= (-4\pi/\eta)\ [C_1 \cos(\beta z) + (1/2)\ V_o \sin(\beta|z|) + U] \end{aligned} \tag{4.8}$$

where

$$U = (-j\eta/4\pi)\ \ {}_{-H}\int^{H} I_z(z')\ K(H,z')\ \ dz' \tag{4.9}$$

and the difference kernel is

$$K_d(z,z') = K(z,z') - K(H,z') \tag{4.10}$$

The constant C_1 can now be expressed in terms of U and V_o by setting Z = H. Since the left hand side of (4.8) vanishes, the right hand side can be solved for C_1 to give

$$C_1 = -\frac{(V_0/2)\sin(\beta H) + U}{\cos(\beta H)} \tag{4.11}$$

If this value of C_1 is substituted in (4.8), the following equation is obtained

$$\int_{-H}^{H} I_z(z')\, K_d(z,z')\, dz' = (4\pi/\eta\cos\beta H)\,[(V_o/2)\sin\beta(H-|z|) + U(\cos\beta z - \cos\beta H)] \tag{4.12}$$

The integral equation (4.12) for the current in a single isolated antenna is readily generalized to apply to the two identical, parallel, and non staggered elements shown in Fig.4.3. It is merely necessary to add to the vector potential on the surface of each element the contributions by the current in the other element. Thus for element 1, the vector potential difference is

$$\begin{aligned} 4\pi\mu^{-1}[A_{1z}(z)-A_{1z}(H)] &= \int_{-H}^{H}[\, I_{1z}(z')\, K_{11d}(z,z') + I_{2z}(z')\, K_{12d}(z,z')]dz' \\ &= (j4\pi/\eta\cos\beta H)\,[(V_{1o}/2)\sin\beta(H-|z|) + U_1(\cos\beta z - \cos\beta H)] \end{aligned} \tag{4.13}$$

Similarly, for element 2

$$4\pi\mu^{-1}[A_{2z}(z)-A_{1z}(H)] = {}_{-H}\int^{H}[I_{1z}(z')\ K_{21d}(z,z')+I_{2z}(z')K_{22d}(z,z')]dz' \quad (4.14)$$

$$(j4\pi/\eta\cos\beta H)[(V_{20}/2)\ \sin\beta(H-|z|)+U_2(\cos\beta z-\cos\beta H)]$$

In these expressions

$$K_{11d}(z,z') = (e^{-j\beta R_{11}}/R_{11}) - (e^{-j\beta R_{11H}}/R_{11H}) = K_{11}(z,z') - K_{11}(H,z') \quad (4.15)$$

$$K_{12d}(z,z') = (e^{-j\beta R_{12}}/R_{12}) - (e^{-j\beta R_{12H}}/R_{12H}) = K_{12}(z,z') - K_{12}(H,z') \quad (4.16)$$

with

$$R_{11} = \sqrt{(z-z')^2+a^2} \qquad R_{11H} = \sqrt{(H-z')^2+a^2}$$
$$R_{12} = \sqrt{(z-z')^2+b^2} \qquad R_{12H} = \sqrt{(H-z')^2+b^2} \quad (4.17)$$

$K_{21}(z,z')$ and $K_{22}(z,z')$ are obtained from the above formulas when the subscripts 1 and 2 are interchanged.

The two simultaneous integral equations (4.13) and (4.14) can be reduced to a single equation if the two driving voltages and the resulting two currents are equal in magnitude but 180° out of phase, i.e .

$$V_{1o} = -V_{2o} = V_1 \quad , \quad I_{1z}(z) = -I_{2z}(z) = I_z(z) \quad (4.18)$$

thus the equations again become alike and equal to

$${}_{-H}\int^{H} I_z(z')\ K_d(z,z')\ dz' = (j4\pi/\eta\cos\beta H)\ [(v_1/2)\ \sin\beta(H-|z|) + U_1(\cos\beta z - \cos\beta H)] \quad (4.19)$$

where

$$U_1 = (-j\eta/4\pi)_{-H}\int^{H} I_z(z')\ K(H,z')\ dz' \quad (4.20)$$

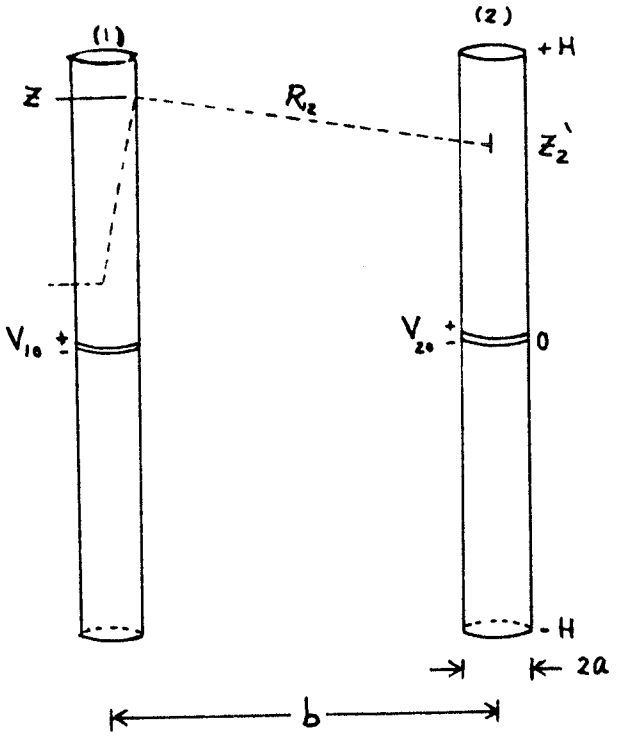

Fig.4.3 : Two identical parallel dipoles .

$$K_d(z,z') = K(z,z') - K(H,z') \tag{4.21}$$

$$K(z,z') = (e^{-j\beta R_{11}}/R_{11}) - (e^{-j\beta R_{12}}/R_{12}) \tag{4.22}$$

The solution of the integral equation can be done using the following approximate representation of the integral in (4.19).

For $\beta b < 1$

$$\int_{-H}^{H} I_z(z')[(\cos\beta R_{12}/R_{12}) - (\cos\beta R_{12H}/R_{12H})]\, dz' = \Psi_{12}(z)\, I_z(z) = \Psi_{12}\, I_z(z) \tag{4.23}$$

where Ψ_{12} is constant

For $\beta b \geqslant 1$

$$\int_{-H}^{H} I_z(z')\, [(\cos\beta R_{12}/R_{12}) - (\cos\beta R_{12H}/R_{12H})]\, dz' \sim \cos\beta z - \cos\beta H \tag{4.24}$$

For all βb

$$\int_{-H}^{H} I_z(z')\, [(\sin\beta R_{12}/R_{12}) - (\sin\beta R_{12H}/R_{12H})]\, dz' \sim \cos(\beta z/2) - \cos(\beta H/2) \tag{4.25}$$

Using (4.23) (4.24) and (4.25), equation (4.19) can be written as

$$I_z(z) = I_v[\sin\beta(H-|z|) + T_v(\cos\beta z - \cos\beta H) \quad T_D(\cos\beta z/2) - \cos(\beta H/2))] \tag{2.26}$$

where I_v , T_v and T_D are complex coefficients which must be determined. The difference between the distribution function ($\cos\beta z$ -

$\cos\beta H$) and ($\cos 1/2\beta z$ - $\cos 1/2\beta H$) is relatively unimportant in the determination of the far field provided that $\beta H < 5\pi/4$. Hence

$$I_z(z) = I_v[\sin\beta(H-|z|) + T(\cos\beta z-\cos\beta H)] \tag{4.27}$$

Substituting (4.27) in (4.19) one obtain

$$I_v = \frac{j2\pi V_1}{\eta\Psi_{dR}\cos\beta H} \tag{4.28}$$

$$T = -\frac{\Psi_v(H) - (\Psi_{d\sum R} + j\,\Psi_{dI})\cos\beta H}{\Psi_U(H) - \Psi_{dU}\cos\beta H} \tag{4.29}$$

where

$$\Psi_{dR} = \Psi_{dR}(z) \quad ,\begin{cases} z=0 & \beta H \leq \pi/2 \\ z = H - \lambda/4 & \beta H > \pi/2 \end{cases} \tag{4.30}$$

$$\Psi_{dR}(z) = \csc\beta(H-|z|)\,{}_{-H}\!\int^{H} \sin\beta(H-|z'|)\; K_{dR}(z,z')\; dz' \tag{4.31}$$

$$\Psi_{d\sum R} = (\cos\beta H-1)^{-1}\;{}_{-H}\!\int^{H} \sin\beta(H-|z'|)\;[(\cos\beta R_{12}/R_{12}) - (\cos\beta R_{12H}/R_{12H})]\; dz' \tag{4.32}$$

$$\Psi_{dI} = [1-\cos(\beta H/2)]^{-1}\;{}_{-H}\!\int^{H} \sin\beta(H-|z'|)\;\; K_{dI}(0,z')\; dz' \tag{4.33}$$

$$\Psi_{dUR} = (1-\cos\beta H)^{-1}\;{}_{-H}\!\int^{H} (\cos\beta z' - \cos\beta H)\; K_{dR}(0,z')\; dz' \tag{4.34}$$

$$\Psi_{dUI} = [1-\cos(\beta H/2)]^{-1}\;{}_{-H}\!\int^{H} (\cos\beta z' - \cos\beta H)\; K_{dI}(0,z')\; dz' \tag{4.35}$$

For each pair of real and imaginary parts, the notation Ψ_d which is equal to $\Psi_{dR}+\Psi_{dI}$ will be used. Also U is defined as

$$U_1 = (-j\eta/4\pi)\ I_v[\Psi_v(H) + T\,\Psi_u(H)] \tag{4.36}$$

$$\Psi_v(H) = \int_{-H}^{H} \sin\beta(H-|z'|)\ K(H,z')\ dz' \tag{4.37}$$

$$\Psi_U(H) = \int_{-H}^{H} (\cos\beta z' - \cos\beta H)\ \ K(H,z')\ \ dz' \tag{4.38}$$

Once the current distribution along each element is determined, the far field pattern can be evaluated.

4.3 CURRENT DISTRIBUTION ALONG THE FEED DIPOLES

It is necessary to determine the current distribution along each dipole in the concentric circular arrays shown in Fig.4.2a, so that the radiation pattern can be evaluated. The analysis used here is concerned exclusively with thin cylindrical conductors all aligned in the z-direction in air so that it suffices to use only the axial component of the vector potential to calculate the current distribution along each dipole. Considering the concentric circular arrays shown in Fig.4.2a, the magnetic potential difference integral equation for the m<u>th</u> element in the k<u>th</u> circle is given by

$$\int_{-H}^{H} \sum_{i=1}^{N} \sum_{l=1}^{2M} I_{zil}(z')\ K_{kmil}(z,z')\ \ dz' = (4j\pi/\eta\ \cos\beta H)\ [\ U_{km}\ F_{oz} + (V_{okm}M_{oz}/2)] \tag{4.39}$$

where

$$F_{oz} = \cos\beta z - \cos\beta H$$
$$M_{oz} = \sin\beta(H - z) \tag{4.40}$$

$$U_{km} = \sum_{i=1}^{N}\sum_{l=1}^{2M} U_{kmil} = (-j\eta/4\pi) \int_{-H}^{H} \sum_{i=1}^{N}\sum_{l=1}^{2M} I_z(z')\, K_{kmil}(z',H)\, dz' \tag{4.41}$$

$$K_{kmild}(z,z') = K_{kmil}(z,z') - K_{kmil}(z,H)$$
$$= (e^{j\beta R_{kmil}}/R_{kmil}) - (e^{j\beta R_{kmilH}}/R_{kmilH}) \tag{4.42}$$

$$R_{kmil} = \sqrt{(z-z')^2 + b^2_{kmil}}$$

Due to circular symmetry and the similar arrangement of the elements around each circle, where the driving point voltages for each circular array are equal in magnitude and have a progressive phase shift of π, the current distribution of m<u>th</u> element on the k<u>th</u> circular array is

$$I_{zim}(z) = (-1)^{m-1} \quad I_z(z) \tag{4.43}$$

Also the driving point voltages are

$$V_{oim} = (-1)^{m-1} \quad V_{oi} \tag{4.44}$$

An approximate solution of the integral equation (4.39) is derived in appendix A and the resultant current distribution is given by

$$I_{zim}(z) = (-1)^{m-1} \{jA_i \sin\beta(H-|z|) + B_i(\cos\beta z - \cos\beta H)\} \tag{4.45}$$

where A_i is a real coefficient when V_{oi} is real and B_i is generally a complex coefficient, as described in Appendix A, and can be evaluated from the geometry of the arrays and the driving point voltag-

es or currents. Once the current distribution along each dipole is known, the radiation pattern can be evaluated as discussed next.

4.4 RADIATION PATTERN

The far field of a dipole of length 2H, situated along z-axis with its center at the origin, is given by

$$E_\theta = (j\omega\mu/4\pi)\ (e^{-j\beta r}/r)\ \int_{-H}^{H} I_z(z')\ e^{j\beta z'\cos\theta}\ \sin\theta\ dz' \tag{4.46}$$

Since the current distribution along any dipole in the concentric circular array is given by (2.4), substitution for I_z (z') leads to

$$E_{\theta i} = (j\omega\mu/4\pi)\ (r^{-j\beta r}/r)\ \{jA_i\ F(\theta,\beta H) + B_i\ G(\theta,\beta H)\} \tag{4.47}$$

where

$$F(\theta,\beta H) = \frac{2}{\beta}\ \frac{\cos(\beta H\ \cos\theta) - \cos\beta H}{\sin\theta} \tag{4.48}$$

$$G(\theta,\beta H) = \frac{2}{\beta}\ \frac{\sin\beta H\ \cos(\beta H\ \cos\theta) - \cos\beta H\ \sin(\beta H\ \cos\theta)}{\sin\theta\ \cos\theta} \tag{4.49}$$

Assuming that the feed array is situated on the bisector of the corner angle, the far field of the kth element and the ith circle of the concentric circular arrays is given by

$$E_\theta = (j\omega\mu/4\pi)\ (e^{-j\beta r}/r)\ \{jA_i\ F(\theta,\beta H) + B_i\ G(\theta,\beta H)\}\ e^{j\beta\rho\ \sin\theta\ \cos(\Phi-\Phi_k)} \tag{4.50}$$

which can be re-written as

$$E_\theta = E_{\theta i}\ e^{j\beta\rho\ \sin\theta\ \cos(\Phi-\Phi_k)} \tag{4.51}$$

The summation of the field from all elements in the concentric circular arrays gives the total far field from the corner array within the corner angle as

$$E_\theta = \sum_{i=1}^{N} \sum_{k=1}^{2M} (-1)^{k-1} \quad E_{\theta i} \qquad e^{j\beta\rho \sin\theta \cos(\Phi-\Phi_k)} \tag{4.52}$$

Again using mathematical identities over the Bessel and trigonometric functions, equation (4.52) can be expanded in an infinite series and the result is given by

$$E_\theta = (4j\eta/\psi)\ (e^{j\beta r}/r) \sum_{n=1}^{\infty} (-1)^{n\pi/\psi} \{ \sum_{i=1}^{N} J_{n\pi/\psi}(\beta\rho_i \sin\theta) \\ [jA_i\ F(\theta,\beta H) + B_i\ G(\theta,\beta H)]\} \ \cos(n\pi\Phi/\psi) \tag{4.53}$$

For the special case of $\beta H = \pi/2$, the expression of the current distribution becomes indeterminate of the form 0/0, so that the formula for the current may be rearranged as shown in appendix A.

While equation (4.53) gives the radiation pattern for the corner array, the effect of the mutual coupling appears in the coefficients A_i and B_i. When using the values of the locations and driving point currents from the design of the corner array in chapter II, we get a slightly different radiation pattern and gain. In this case some adjustment of the driving point currents should be introduced to obtain optimum 1 described in chapter II.

For the calculation of the coefficients A_i and B_i, a computer program was prepared using the formulation described in appendix A. Then the results for A_i and B_i were compared with those given in [17] for one circular array indicating a good agreement. Also the

program was designed to satisfy two requirements. First when the locations of the elements and the driving point currents are specified, the program evaluates the corresponding pattern and gain . This gives an indication about the change in the pattern and gain when the design in chapter II is used and mutual coupling is involved in the solution. Second, if the locations are specified, the program includes the Dolph Tchebyscheff technique to calculate new driving currents at a specific main to sidelobe level (i.e optimum 1) as described in chapter II. In this case one can evaluate the required modification in the currents given in the design of chapter II. Also the calculation of the mutual coupling coefficients A_i and B_i is generalized and applied to the off-axis case.

4.5 RESULTS AND DISCUSSION

Radiation patterns and gain are calculated for four cases with the mutual coupling involved in the solution. Each case is treated by two methods. First, the design parameters given in chapter II and III (for optimum 1) are used for the calculation of the pattern and gain taking the mutual coupling into account. Of course this no longer gives optimum 1 , but it gives an indication of the effect of mutual coupling on the pattern and gain of the designs given in the last two chapters. This method will be denoted by method 1. Second, a modification of the exciting currents is done to generate optimum 1 again for each case keeping the other design parameters as given in the last two chapters. This method will be denoted by method 2 . The excited dipoles are assumed to be half wave dipoles with a radius of 0.002λ .

Fig.4.4 gives a comparison between the radiation patterns corresponding to method 1 and method 2 for Schell's case. As can be seen in this first case, the effect of mutual coupling appears in the sidelobes which increase over the case where mutual coupling is neglected. The design parameters and resulting radiation characteristics corresponding to the two methods are given in Table 4.1. As seen from Table 4.1, a slight change in the gain and beamwidth occurs before and after the modification of the exciting currents.

The second case is the equispaced feed array case described in chapter II. The patterns for this case, for the two methods, are shown in Fig. 4.5. An increase in the first sidelobe level by 1.1 dB has occurred due to mutual coupling. Very small changes in the gain and the beamwidth due to the mutual coupling are also noted as shown in Table 4.2. Also, the modified exciting currents are given in Table 4.2, which show a slight difference in magnitudes but a large difference in phase compared to method 1. In this case the effect of mutual coupling on the radiation pattern is small due to the relatively large spacing between the feed dipoles.

The third case under consideration is the unequispaced feed array given in chapter II (optimum 1). Here it is observed that the difference between the radiation patterns of the two methods described above is relatively large. As seen in Fig. 4.6, the first sidelobe level is decreased by 2.31 dB when the mutual coupling is taken into account, while the null to null width is increased by approximately 2°. Table 4.3 gives a comparison of the designs giv-

en in chapter II and the modified design. As can be seen, slight modifications in the exciting currents may generate optimum 1 again. From this case we conclude that the locations of the feed array with respect to each other have a large effect when the mutual coupling is involved.

In the fourth case, as can be seen from Fig. 4.7, the radiation patterns for the off axis case are almost exactly the same with and without mutual coupling. This is due to the symmetrical arrangement of the feed dipoles with respect to the axis of the reflector. A comparison between the radiation characteristics with and without mutual coupling gives 0.35 dB increase in the first sidelobe level and the same gain and beamwidth when mutual coupling is introduced. This case shows a negligible effect of mutual coupling on the radiation characteristics.

Another iterative search is done to calculate the design parameters which give the highest gain irrespective of the side lobe level (optimum 2) when mutual coupling is involved in the solution. In this search the locations are adjusted, as well as the exciting currents. The results obtained corresponding to this optimum case are shown in Table 4.4. Fig.4.8 gives the corresponding radiation pattern. The gain is found to be 20.08 dB which is the highest gain obtained for the 60° corner array. As shown in Fig.4.9, the first sidelobe level is -24.945 dB while the second sidelobe level is -13.5 dB, and the beamwidth is 10.08°. From this case we see that the mutual coupling effect could be helpful in increasing the gain of this antenna if the sidelobe level is not required to be low.

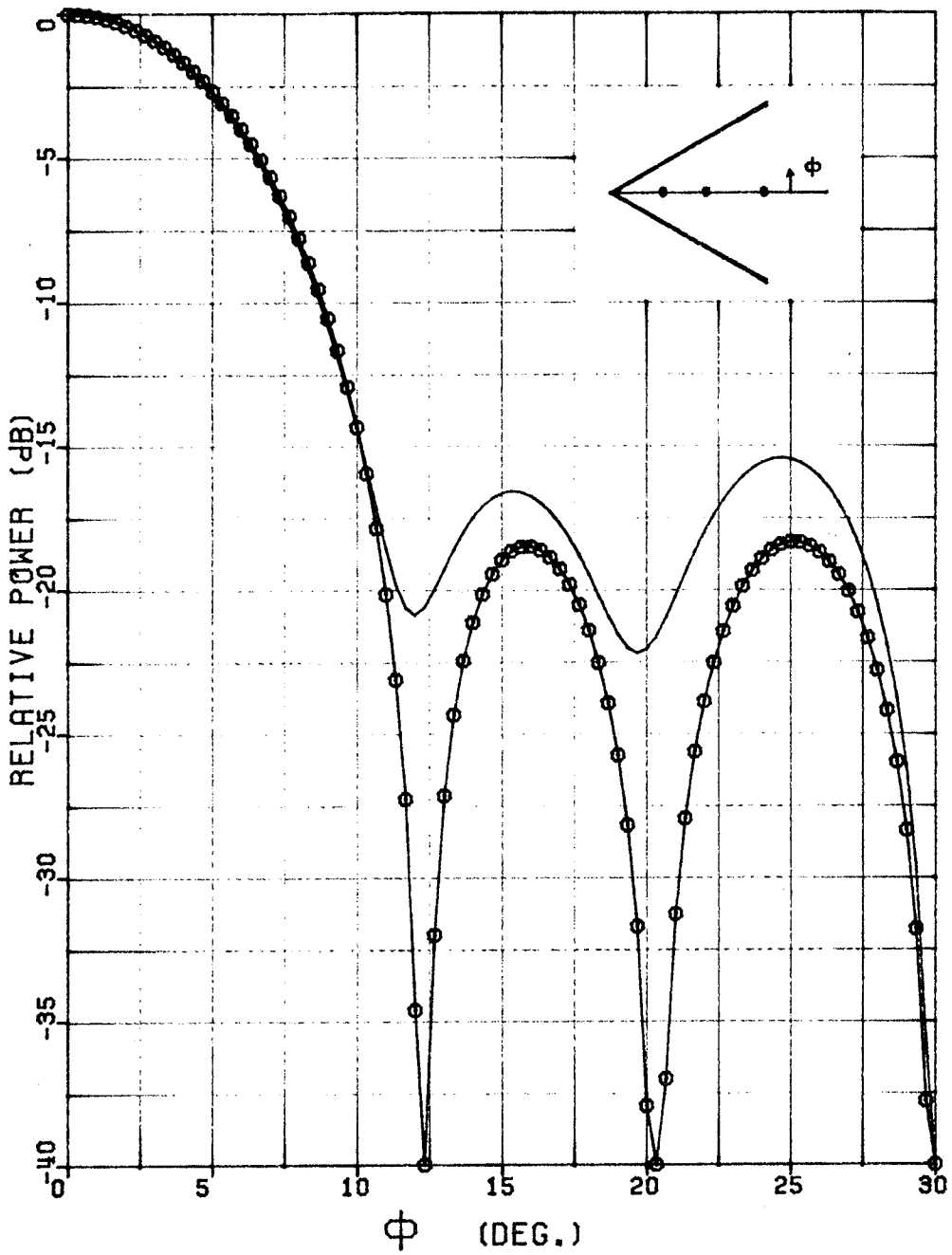

FIG.4.4: RADIATION PATTERN FOR SCHELL CASE

— METHOD 1

⊖⊖⊖ METHOD 2

TABLE 4.1

Design Parameter and Radiation Characteristics of Schell Case (ψ=60° 3-driven elements)

	Method 1			Method 2		
	Element (1)	Element (2)	Element (3)	Element (1)	Element (2)	Element (3)
$\lvert I \rvert$	0.775	1.250	1.000	0.935	1.450	1.000
θ	0.000	180.0	0.000	14.50	179.2	0.000
ρ/λ	0.640	1.580	2.740	0.640	1.580	2.740
Gain (dB)	16.99			16.88		
B.W. (Deg.)	10.33			10.49		
R (dB)	16.59			18.50		

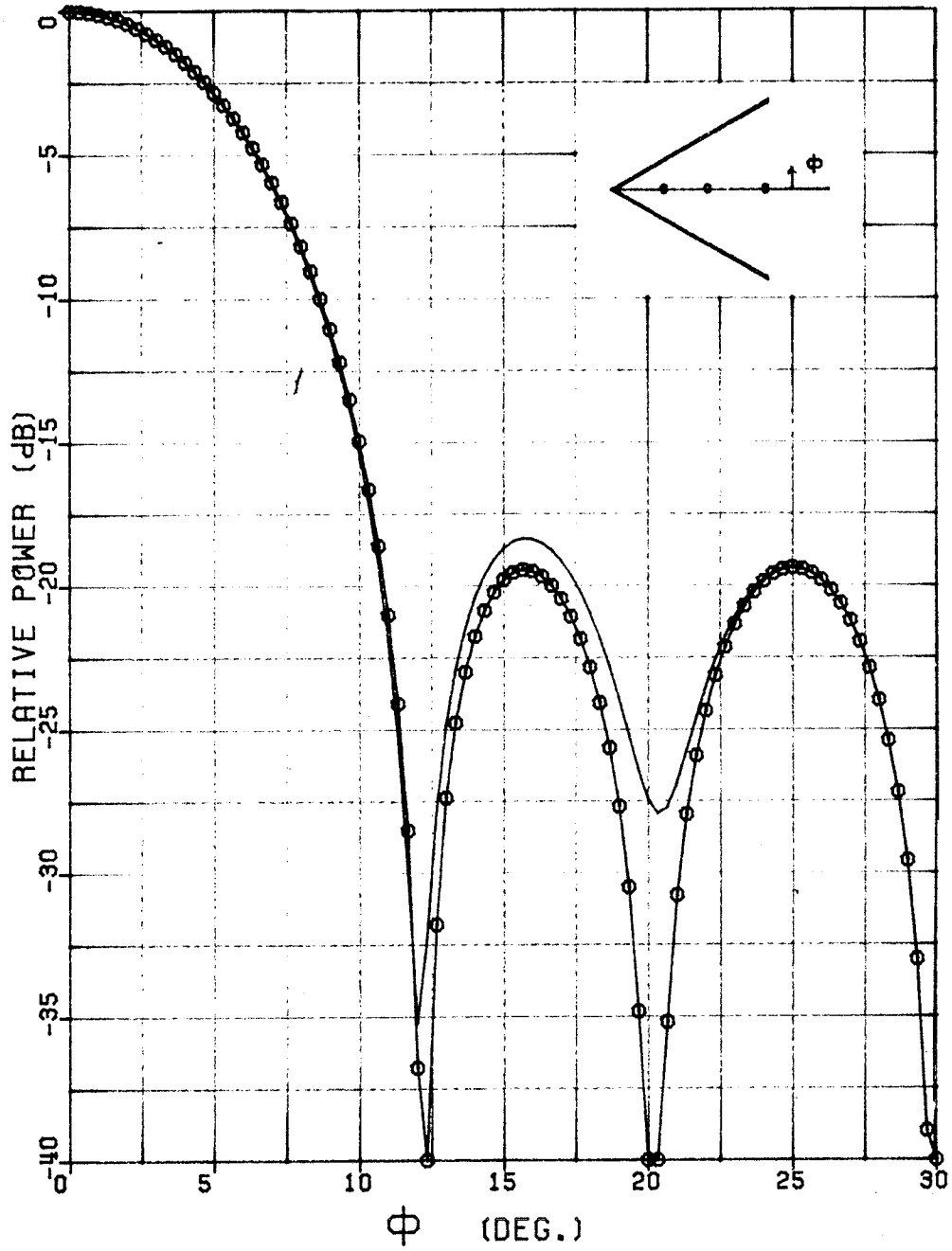

FIG.4.5: RADIATION PATTERN FOR

CASE 1

— METHOD 1

METHOD 2

TABLE 4.2

Design Parameter and Radiation Characteristics of Case 1 (ψ=60° 3-driven elements)

	Method 1			Method 2		
	Element (1)	Element (2)	Element (3)	Element (1)	Element (2)	Element (3)
$\lvert I \rvert$	1.000	0.130	0.180	1.000	0.133	0.174
θ	0.000	180.0	0.000	00.00	-154.6	9.250
ρ/λ	0.240	1.380	2.520	0.240	1.380	2.520
Gain (dB)	18.93			18.94		
B.W. (Deg.)	10.17			10.23		
R (dB)	18.34			19.45		

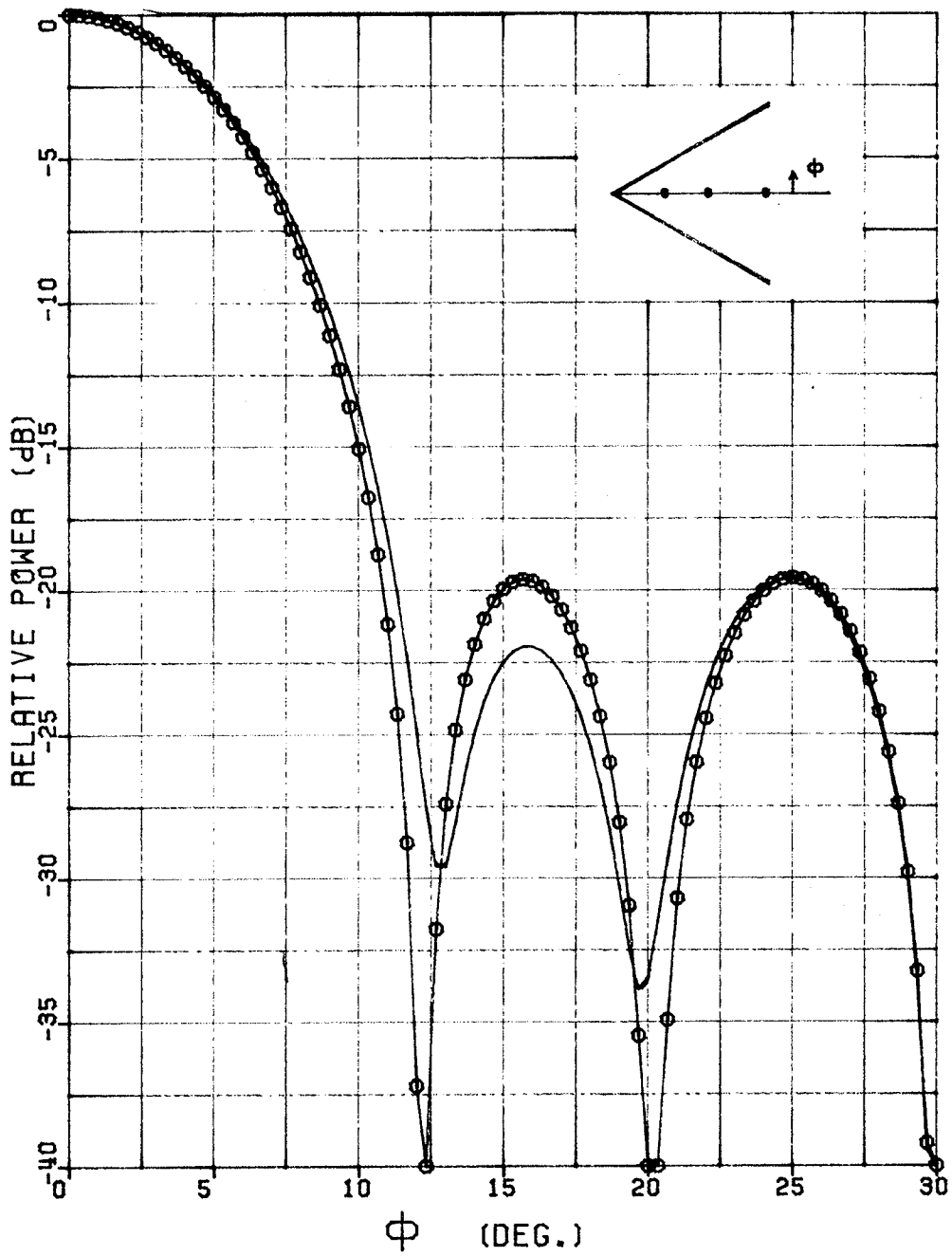

FIG.4.6: RADIATION PATTERN FOR CASE 2

— METHOD 1

⊖⊖⊖ METHOD 2

TABLE 4.3

Design Parameter and Radiation Characteristics of Case 2 (ψ=60° 3-driven elements)

	Method 1			Method 2		
	Element (1)	Element (2)	Element (3)	Element (1)	Element (2)	Element (3)
$\|I\|$	1.000	0.336	0.300	1.000	0.303	0.313
θ	0.000	180.0	0.000	00.00	-174.9	5.870
ρ/λ	0.300	1.100	2.433	0.300	1.100	2.433
Gain (dB)	19.618			19.683		
B.W. (Deg.)	10.445			10.19		
R (dB)	21.92			19.61		

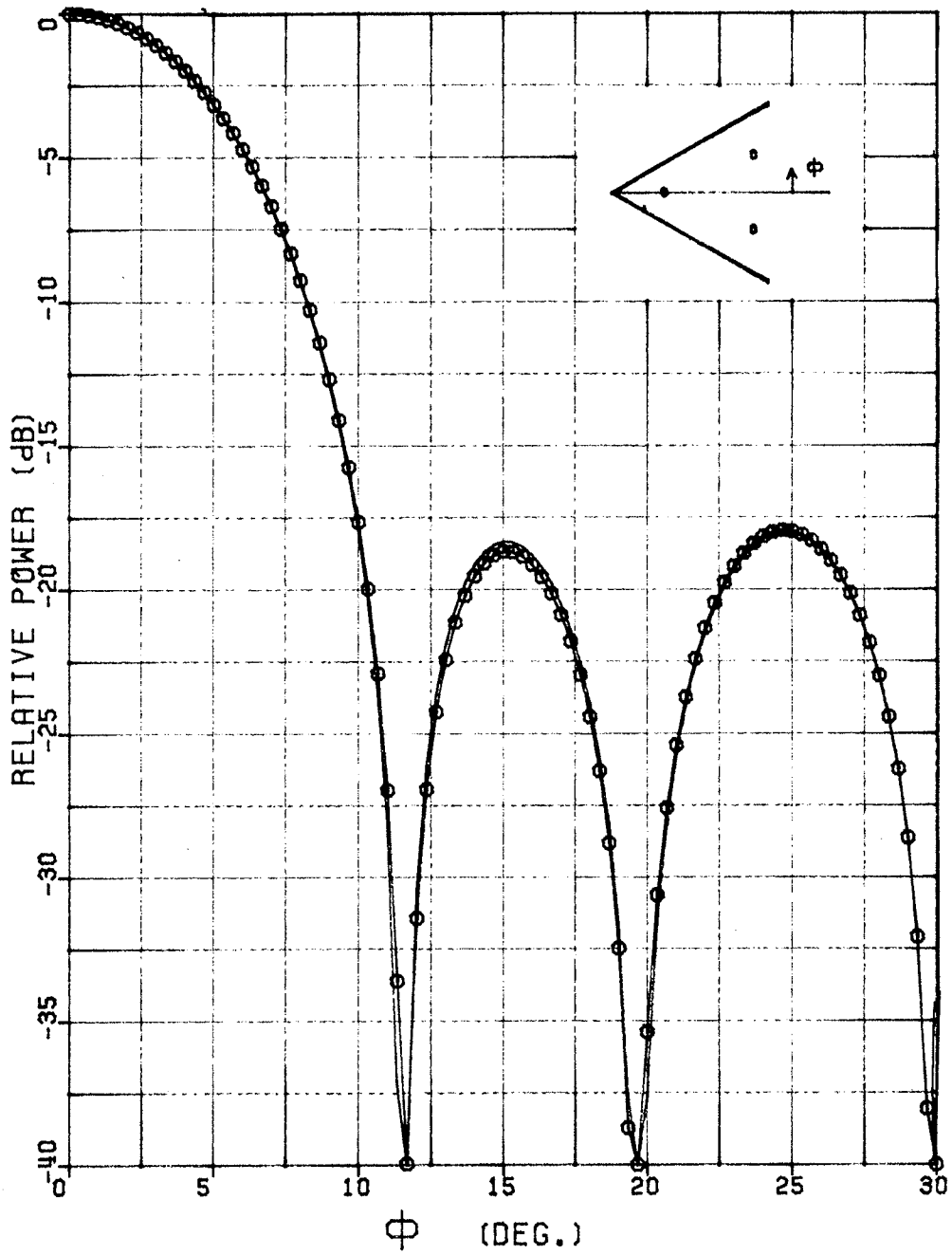

FIG.4.7: RADIATION PATTERN FOR

CASE 3

—— WITHOUT COUPLING

WITH COUPLING

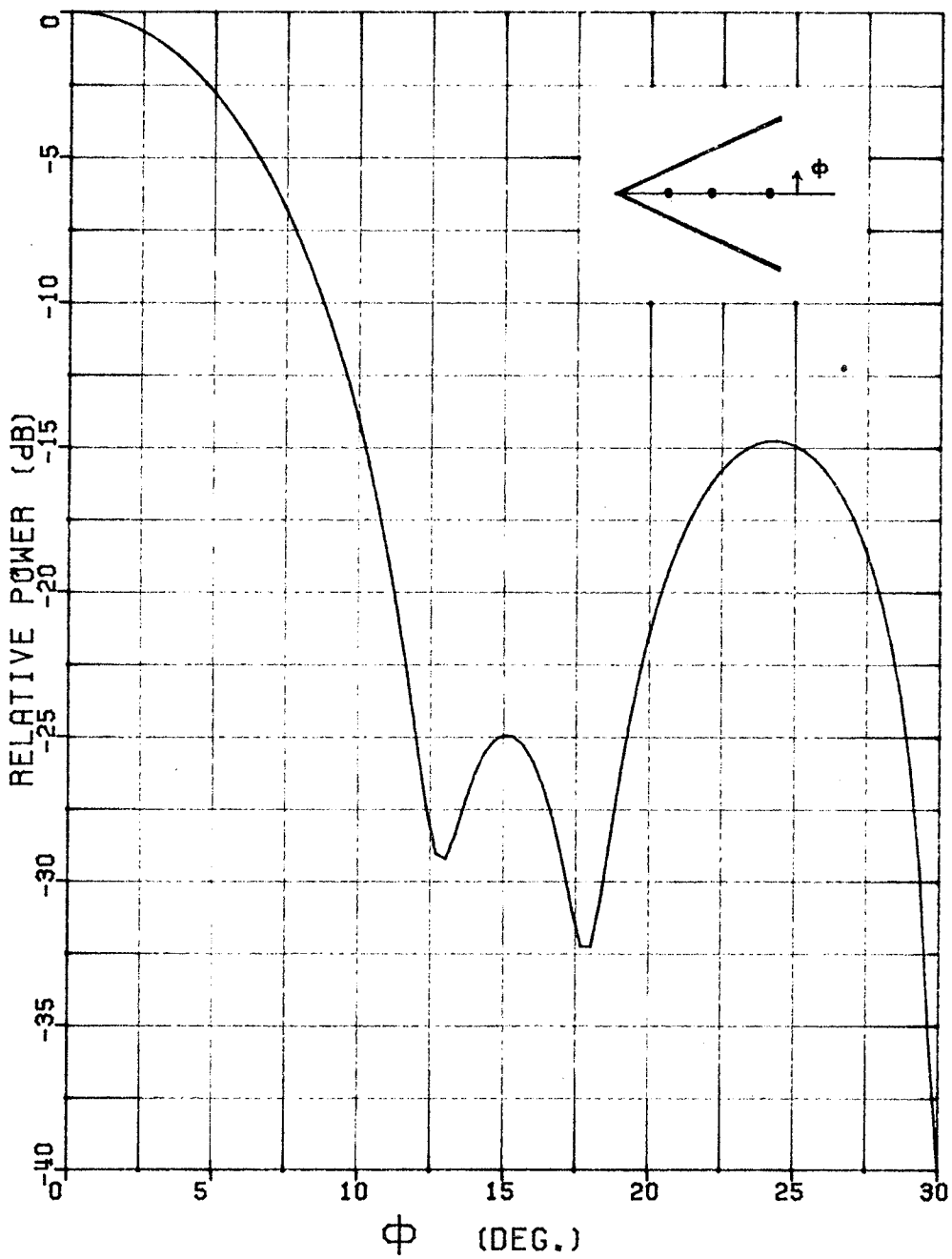

FIG.4.8: RADIATION PATTERN FOR OPTIMUM 2

TABLE 4.4

Design Parameter and Radiation Characteristics of highest Gain Case (ψ=60° 3-driven elements)

	Element (1)	Element (2)	Element (3)
$\|I\|$	1.000	0.463	0.366
θ	0.000	180.0	0.000
ρ/λ	0.420	0.900	2.480
Gain (dB)	20.084		
B.W. (Deg.)	10.245		
R (dB)	24.95		

Chapter V

EDGE DIFFRACTION EFFECT

5.1 INTRODUCTION

In the preceding chapters, the solution of the corner array is given for a semi-infinite reflector length. In order to deal with a practical (finite) reflector length of the corner array, the effect on the radiation characteristics of diffraction from the reflector edges must be taken into account.

Two methods of analysis are used for the evaluation of the far field radiation pattern. First is the integral equation formulation method, in which the far field is attributed to the feed array in isolation in addition to the current density which is induced on the reflector surface. In this method the feed array is considered as an array of infinite line sources positioned anywhere between two perfectly conducting surfaces of finite length and arbitrary corner angle as shown in Fig.5.1. Second, the geometrical theory of diffraction is employed for the same configuration. In the latter method, the total space is divided into regions, as will be described later, and the far field radiation pattern due to the sources, as well as images of the sources and the edge images are calculated.

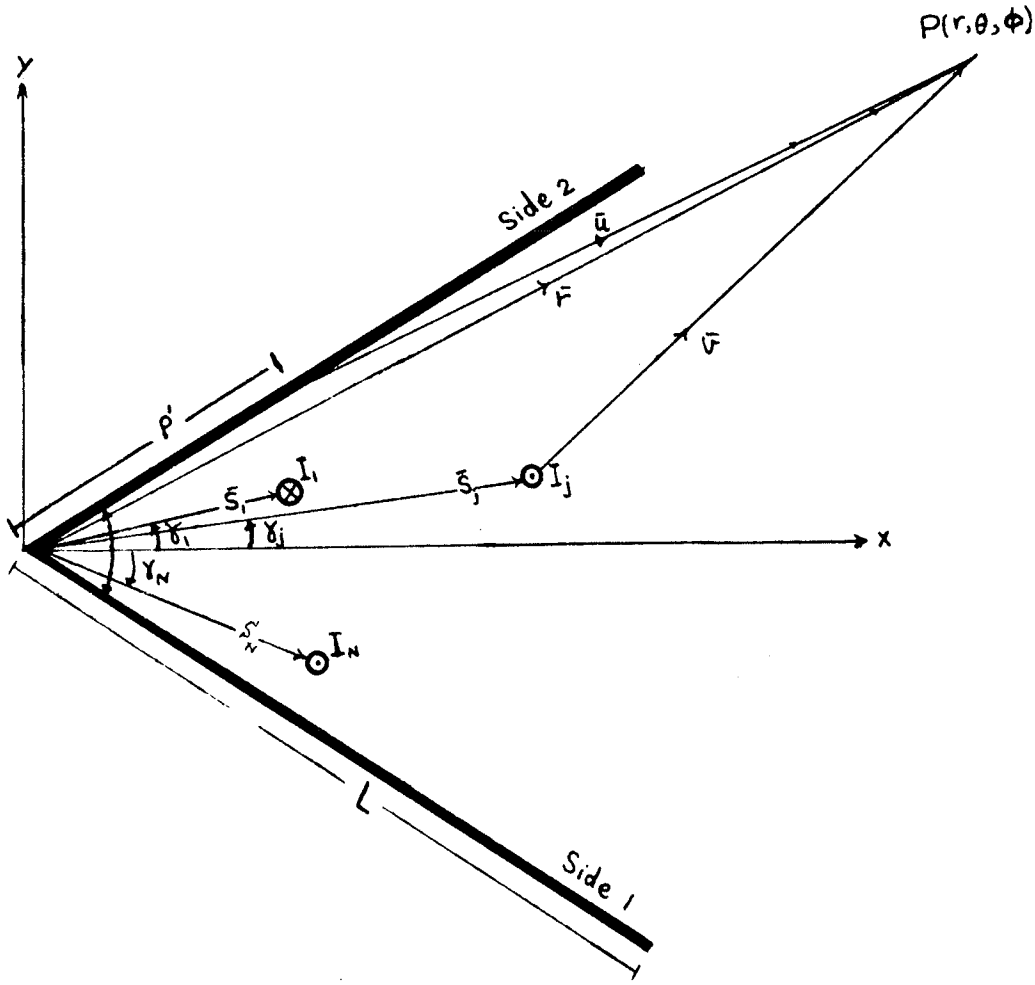

Fig.5.1 : Schematic diagram of corner array.
(finite wall length)

5.2 INTEGRAL EQUATION FORMULATION

From the time harmonic Maxwell's equations, one can derive the homogeneous wave equation [23]

$$\nabla^2\Psi(\bar{\rho}) + \beta^2\Psi(\bar{\rho}) = 0 \tag{5.1}$$

where $\Psi(\bar{\rho})$ represents either the electric or the magnetic field and β is the wave number.

For the corner array considered in this chapter, there will be no variation of $\Psi(\bar{\rho})$ in the z direction. Thus, one is concerned with the two-dimensional Laplacian operator and a two-dimensional space (x-y plane).

Referring to Fig.5.2 the wave equation of an infinite line source of unit intensity may be expressed in terms of the Green's function as [24]

$$\nabla^2 G(\bar{\rho},\bar{\rho}') + \beta^2 G(\bar{\rho},\bar{\rho}') = \delta(\bar{\rho}-\bar{\rho}') \tag{5.2}$$

Equation (4.2) has the well known solution

$$G(\bar{\rho},\bar{\rho}') = (-1/4j)\ H_o^{(2)}(\beta\,|\bar{\rho}-\bar{\rho}'|) \tag{5.3}$$

Upon using equation (5.2) and the Green's second identity

$$\oint_s (G\ \partial\Psi/\partial n - \Psi\ \partial G/\partial n)\ dS = \int_v (\Psi\nabla^2 G - G\nabla^2\Psi)\ dv \tag{5.4}$$

equation (5.1) can be solved for Ψ by multiplying equation (5.1) by G and equation (5.2) by Ψ and subtracting. In so doing, we get

$$\Psi(\bar{\rho})\nabla^2 G(\bar{\rho},\bar{\rho}') - G(\bar{\rho},\bar{\rho}')\nabla^2\Psi(\bar{\rho}) = \Psi(\bar{\rho})\ \delta(\bar{\rho}-\bar{\rho}') \tag{5.5}$$

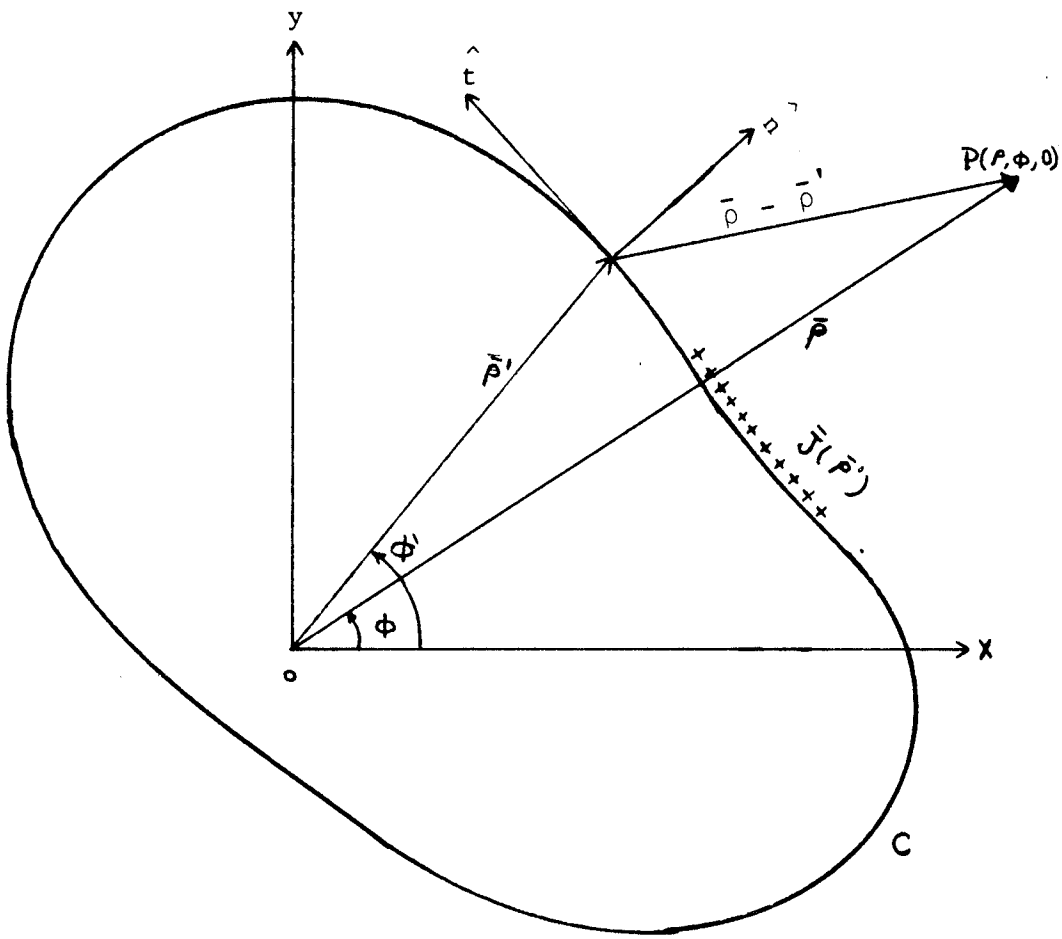

Fig.5.2 : Schematic diagram of the closed surface.

(Two dimension)

Substituting equation (5.5) into (5.4) and using the property of the Delta function, the solution of (5.1) in two dimensions is given by

$$\Psi(\bar{\rho}) = {}_c\oint \Psi(\bar{\rho}')\ \partial G(\bar{\rho},\bar{\rho}')/\partial n\ d\rho' - {}_c\oint G(\bar{\rho},\bar{\rho}')\ \partial\Psi(\bar{\rho}')/\partial n\ d\rho' \quad (5.6)$$

where $\bar{\rho}$, $\bar{\rho}'$ and C are illustrated in Fig.5.1

For the transverse magnetic (TM) solution, the scalar function $\Psi(\bar{\rho})$ is associated with the E_z component of the field. By an application of Maxwell's curl equation for $\bar{H}$, one finds that the tangential component of the field H_T is as follows

$$\bar{H}_T = (-j/\omega\mu)\ \partial\Psi/\partial n\ \hat{t} \quad (5.7)$$

These field components may then be related to the equivalent surface current densities by:

$$\bar{M} = \bar{E} \times \hat{n}$$

and (5.8)

$$\bar{J} = \hat{n} \times \bar{H}$$

Thus, one finds that,

$$M(\bar{\rho}) = \Psi(\bar{\rho})\ \hat{t}$$

$$J(\bar{\rho}) = (-j/\omega\mu)\ \partial\Psi(\bar{\rho})/\partial n\ \hat{z} \quad (5.9)$$

Upon substituting (5.9) into (5.6), one gets

$$E_z = {}_c\oint M(\bar{\rho}')\ \partial G(\bar{\rho},\bar{\rho}')/\partial n\ d\rho' - j\omega\mu\,{}_c\oint J_z(\bar{\rho}')\ G\ (\bar{\rho},\bar{\rho}')\ d\rho' \quad (5.10)$$

Equation (5.9) is the general formula for the scattered E_z field due to the equivalent magnetic and electric current sources.

On a perfectly conducting surface the total tangential E_z field, which is the sum of the incident as well as the scattered field, must be equal to zero, i.e,

$$E_z(\vec{\rho}') = E_z^i(\bar{\rho}') + E_z^s(\bar{\rho}') = 0 \tag{5.11}$$

also the magnetic current $\bar{M}(\bar{\rho}')$ equals zero on the perfectly conducting surface. Applying equation (5.9) with the boundary conditions described above on the reflector surface of the corner array, one gets

$$E_z^s(\bar{\rho}') = - E_z^i(\bar{\rho}') = (-\omega\mu/4) \int_{\substack{\text{reflector}\\ \text{arc}}} J_z(\bar{\rho}') \, H_o^{(2)}(\beta\,|\bar{\rho}-\bar{\rho}'|) \, dL' \tag{5.12}$$

The integral equation (5.12) is of the form of a Fredholm integral equation of the first kind, where the Hankel function is the kernel of the equation and the current density $J(\bar{\rho}')$ is the unknown. The incident electric field E_z^i is a known excitation function due to the array of line sources and is given by.

$$E_z(\bar{\rho}) = \sum_{j=1}^{N} -\mu\omega/4 \; I_j \, H_o^{(2)}(\beta\,|\bar{\rho}-\bar{s}_j|) \tag{5.13}$$

Now, the solution of (5.12) with (5.13) can be carried out using the method of moments [25] as will be shown next.

5.2.1 Solution Of The Integral Equation Formulation

The reflector length can be divided into N unequal segments. The segments at the edges and the corner are smaller than those at the middle of the arc length. The current density J_z $(\bar{\rho}')$ can be represented as

$$J_z = \sum_{n=1}^{N} \alpha_n f_n \tag{5.14}$$

where f_n is the basis function described by

$$f_n(\rho) = \begin{cases} 1 & \text{over } \Delta c_n \\ 0 & \text{elsewhere} \end{cases} \tag{5.15}$$

and α_n are the unknown coefficients, while ΔC_n is the n<u>th</u> segment length of the reflector arc. Substituting equation (5.14) into (5.12), the result can be written as

$$[L_{mn}]\,[\alpha_n] = [g_m] \tag{5.16}$$

where

$$\begin{aligned} L_{mn} &= (-\omega\mu/4) \int_{\Delta c_n} H_0^{(2)}(\beta\,|\bar{\rho}_m - \bar{\rho}_n'|)\, dL' \\ &= (-\omega\mu/4)\, \Delta c_n\, H_0^{(2)}(\beta\,|\bar{\rho}_m - \bar{\rho}_n|) \end{aligned} \tag{5.17}$$

This approximation is valid whenever the two integers m and n are not equal. However, for the diagonal element L_{nn} the small argument representation of the Hankel function is employed. This leads to

$$L_{nn} = (\omega\mu/4)\, \Delta c_n\, [1 - j\,(2/\pi)\,(\gamma + \ln(\beta \Delta c_n/4e))] \tag{5.18}$$

where γ=0.5772 (Euler's constant). The excitation g_m can be evaluated from

$$g_m = \sum_{j=1}^{N} (-\mu\omega/4)\ I_j\ H_o^{(2)}(\beta\,|\bar{\rho} - \bar{s}_j|) \tag{5.19}$$

Once the current density is evaluated, the far field radiation pattern can be evaluated as outlined next.

5.2.2 Radiation Pattern

The far field radiation pattern $F(\Phi)$ resulting at each observation point p is the sum of the field from the current on the reflector surface J and the field from the excited array sources. Therefore, $F(\Phi)$ can be represented as

$$F(\Phi) = \sum_{j=1}^{N} (-\omega\mu/4)\ I_j\ H_o^{(2)}(\beta v_j) - (\omega\mu/4) \int_{\substack{\text{reflector}\\ \text{arc}}} J_z(\bar{\rho}')\ H_o^{(2)}(\beta u)\ dL' \tag{5.20}$$

where Φ is the observation angle while v_j and u are shown in Fig.5.1. For the phase terms one can assume that

$$\begin{aligned} v &= r - s_j \cos(\Phi - \gamma_j) \\ u &= r - \rho' \cos(\Psi/2 - \Phi) \qquad \text{,for reflector side 1} \\ u &= r - \rho' \cos(\Psi/2 + \Phi) \qquad \text{,for reflector side 2} \end{aligned} \tag{5.21}$$

Whereas, for the amplitude terms the distances v_j, and u are considered equal to r. Furthermore, considering the large argument approximation for the Hankel function, equation (5.20) may be rewritten as

$$\begin{aligned} F(\Phi) = \sum_{j=1}^{N} (-\mu\omega/4)\ I_j\ \sqrt{2j/\pi\beta r}\ \ e^{-j\beta r}\ e^{j\beta s_j \cos(\Phi-\gamma_j)} - (\omega\mu/4)\sqrt{2j/\pi\beta r} \\ e^{-j\beta r} \Big\{ \int_{\substack{\text{reflector}\\ \text{side1}}} J(\bar{\rho}')\ \ e^{j\beta\rho\cos(\Psi/2-\Phi)} dL' + \int_{\substack{\text{reflector}\\ \text{side2}}} J(\bar{\rho}')\ e^{j\beta\rho\cos(\Psi/2+\Phi)} dL' \Big\} \end{aligned} \tag{5.22}$$

Dividing by $-\sqrt{2j/\pi\beta r}\ e^{-j\beta r}$ for pattern normalization, one gets

$$F(\Phi) = \sum_{j=1}^{N} (-\mu\omega/4)\ I_j\ e^{j\beta s_j \cos(\Phi-\gamma_j)} + (\omega\mu/4)$$

$$\left\{ \int_{\substack{\text{reflector}\\ \text{side 1}}} J(\bar{\rho}')\ e^{j\beta\rho\cos(\Psi/2-\Phi)} dL' + \int_{\substack{\text{reflector}\\ \text{side 2}}} J(\bar{\rho}')\ e^{j\beta\rho\cos(\Psi/2+\Phi)} dL' \right\} \tag{5.23}$$

Equation (5.22) gives the far field radiation pattern for the corner array in the plane normal to z axis.

5.3 FORMULATION BY THE GEOMETRICAL THEORY OF DIFFRACTION

Ohba's analysis [6] of the corner reflector antenna by the geometrical theory of diffraction can be extended to the solution of a corner array with finite reflector length. Fig. 5.3 shows a schematic diagram of a single source, 60° corner angle, with the images of the source labelled by numbers 2 to 6 and edge images labelled by A_1, A_2, B_1 and B_2. The entire space is divided into 22 regions by planes which contain the dipole and edge, an image of the dipole and edge, an edge and edge image, or two edges. It should be mentioned that the diagrams for the other sources in the feed array can be drawn in a similar manner and the resulting regions will be taken into consideration. Also, the consideration is taken to keep the reflector length at least equal to twice the distance between the apex and the farthest dipole. This makes the sequence of the regions the same for all array sources provided that the boundary angles are changed. The z-component of the Hertzian vector in each region is calculated as described in [6] for one feed source.

Fig.5.3 : Diagram of images and edge images of 60° corner reflector.
(Space is divided into 22 regions)

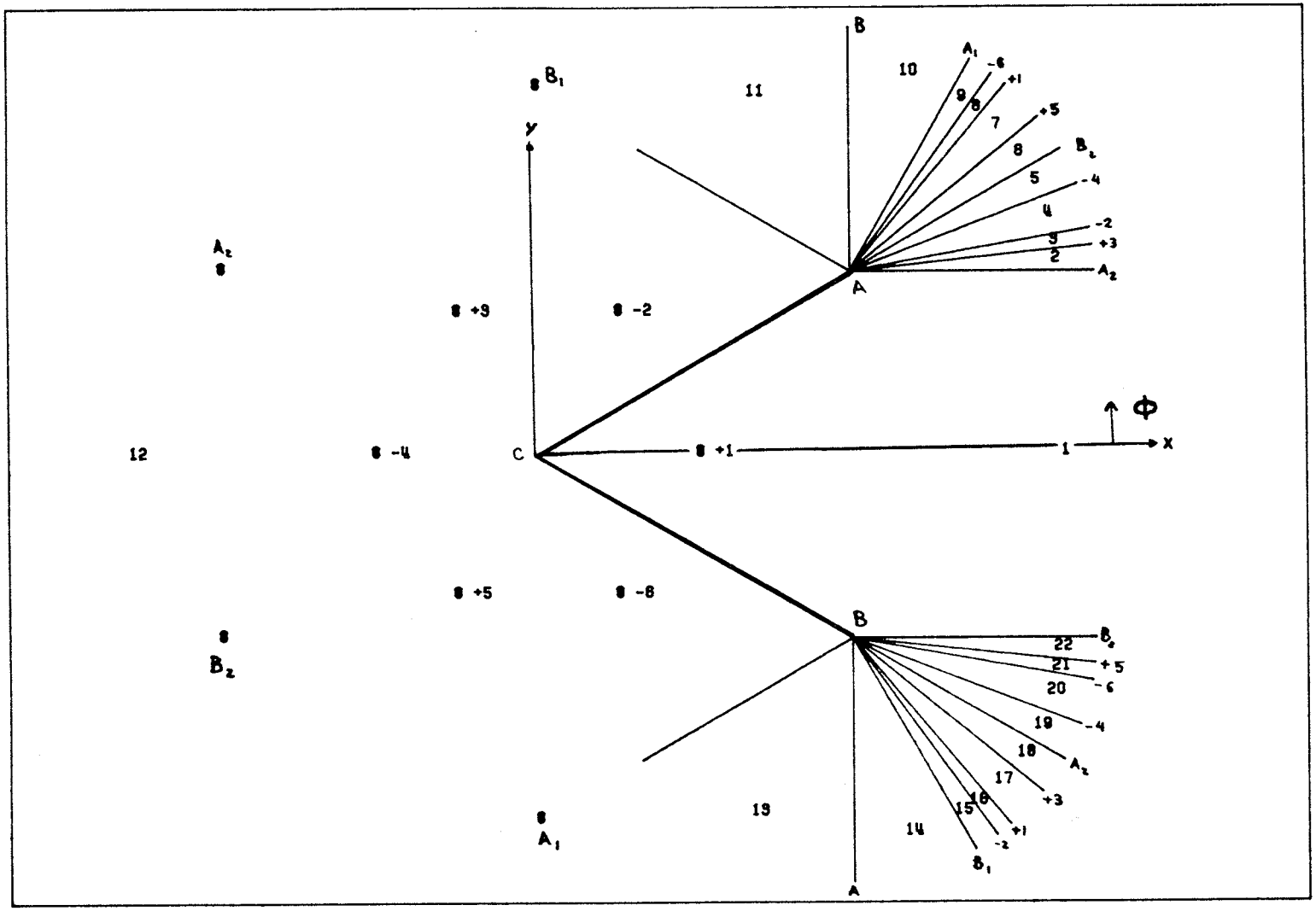

Once the Hertzian vector is evaluated, the far field pattern in each region can be calculated and also extended to the case of the corner array as shown next.

5.3.1 Radiation Pattern

For the observation point P located in region 1, the Hertzian vector due to one source feed in this region is given by

$$\begin{aligned}\pi_z = {} & I_1 - I_2 + I_3 - I_4 + I_5 - I_6 \\ & - I_{1A} + I_{2A} - I_{3A} + I_{4A} - I_{5A} + I_{6A} \\ & - I_{1B} + I_{2B} - I_{3B} + I_{4B} - I_{5B} + I_{6B} \\ & - I_{1A2} + I_{2A2} - I_{3A2} + I_{4A2} - I_{5A2} + I_{6A2} \\ & - I_{1B2} + I_{2B2} - I_{3B2} + I_{4B2} - I_{5B2} + I_{6B2}\end{aligned} \tag{5.24}$$

Where I_n is the direct wave from the dipole and the waves reflected by the conducting plate ABC and is given by

$$I_n = \frac{e^{-j\beta R_n}}{R_n} \qquad ,n=1,2,\ldots\ldots,6 \tag{5.25}$$

R_n is the distance between the dipole or an image and P. I_{nA} or I_{nB} denote the singly diffracted waves from the edges A or B, respectively, after n reflections, and is given by

$$I_{nA} = \frac{e^{-j\beta R_{nA}}}{R_{nA}} \; f(T_{nA}) \tag{5.26}$$

where

$$T_{nA} = \beta(R_{nA} - R_n)$$

$$f(T) = (1/\sqrt{\pi}) \; e^{j(\pi/4)+jT^2} \int_T^{\infty} e^{-jt^2} dt = (1/2)\, e^{jT^2} X(T) \tag{5.27}$$

$$X(T) = \{1 - C(T) - S(T)\} + j\{S(T) - C(T)\}$$

C(T) and S(T) are Fresnel cosine and sine functions, and R_{nA} is the distance between the dipole or the image and the edge plus the distance from the edge to the point P. The term I_{nA2}, or I_{nB2} is due to the waves reflected either from the plates BC or AC after diffraction by edge A or B (i.e. reflections following the edgewaves). For this case the two images of the edges A and B with respect to BC and AC, respectively, must be considered and they are labelled A_1 and B_1. Moreover, the images of A_1 and B_1 with respect to AC and BC are taken into account as A_2 and B_2. Hence I_{nA2} or I_{nB2} is given by

$$I_{nA2} = \frac{e^{-j\beta R_{nA2}}}{R_{nA2}} f(T_{nA2}) \tag{5.28}$$

where

$$T_{nA2} = \beta(R_{nA2} - R_n)$$

and R_{nA2} is the distance between the source or the image and the edge image A_2 plus the distance between A_2 and P. Substituting from (5.25), (5.26), (5.27) into (5.24) one can get

$$E/E_c = \sum_{n=1}^{N} (-1)^{n-1} \; e^{j\beta s \cos(\Phi-(n-1)\pi/3)} \; F(n) \tag{5.29}$$

where

$$F(n) = 1 - (1/2)\,\{X(T_{nA}) + X(T_{nB}) + X(T_{nA2}) + X(T_{nB2})\} \tag{5.30}$$

and

$$E_c = \frac{e^{j\beta r}}{r} \tag{5.31}$$

Equation (5.25) can be extended to give the total far electric field in region 1 for all elements of the feed array, as

$$E_{total}/E_c = \sum_{\ell=1}^{N} I_\ell \sum_{n=1}^{6} (-1)^{n-1} e^{j\beta S_\ell \cos(\phi-(n-1)\pi/3)} F_1^{(\ell)}(n) \tag{5.32}$$

where

$$F_1^{(\ell)}(n) = 1 - (1/2)\{X(T_{nA}^{(\ell)}) + X(T_{nB}^{(\ell)}) + X(T_{nA2}^{(\ell)}) + X(T_{nB2}^{(\ell)})\} \tag{5.33}$$

and where the subscript (ℓ) refers to ℓth element. Moreover the far field in all other regions can be evaluated by the same procedure and the results are shown in appendix B.

5.4 COMPUTER PROGRAMS

Two computer programs were prepared to calculate the radiation pattern using the formulation described above. For the integral equation formulation (I.E.F) the program was designed to solve the integral equation for the current distribution on the reflector surface by employing the method of moments. Since in our problem the reflector length L is relatively long, the reflector arc was divided into 150 segments. For this reason the computation time required for the evaluation of the current density is relatively long , but it gives a good computational accuracy. Once the current distribution on the reflector surface is evaluated, the far field radiation pattern may be calculated using equation (5.23).

Another program was prepared to calculate the radiation pattern using the geometrical theory of diffraction method (G.T.D). As described above, the total space should be divided into 22 regions

for a 60° corner angle and one source feed as shown in Fig.5.4. However, those regions are symmetrically arranged around the axis of the reflector. In this case it is sufficient to calculate the pattern in the regions above the axis in order to save computation time. The space division process is included in the program for each source of the feed array. Once the space is divided, the pattern in each region may be calculated using the formulation described in appendix B. Using AMDAHAL 5850 V/8 computer the computation time for the G.T.D method was 13 seconds, while for the I.E.F method it was 54 seconds.

1.5 RESULTS AND DISCUSSION

The effect of edge diffraction on the radiation pattern is investigated for four different structures. First, the radiation pattern corresponding to the design parameters in Schell's case, as given in chapter II, is evaluated using both I.E.F and G.T.D methods. Fig.5.4 gives the radiation patterns corresponding to both methods. The largest deviation between the two patterns is 0.5 dB in the sidelobe region which indicates a good agreement. It is found that the optimum main to sidelobe level occurs for a reflector length of 7.1λ. The first sidelobe level is found to be lower than the result based on image theory by 2.35 dB while the beamwidth decreases by 0.5°.

Second, for the case of an equispaced feed array the solution by the I.E.F and the G.T.D gives the radiation patterns presented in Fig.5.5, which shows a good agreement between both solutions.

The first sidelobe level corresponding to this case is 1.7 dB lower than that based on the solution by image theory. Also the beamwidth is lower by 0.13 than that based on image theory. The optimum reflector length, corresponding to the lowest sidelobe level, was found to be 6.7λ.

The third case considered is that of the unequispaced feed array given in chapter II. The radiation pattern corresponding to the design parameters given in chapter II is given in Fig.5.6 for both the I.E.F and G.T.D methods. The first sidelobe level has the lowest value corresponding to a reflector length of 6.8λ. As can be seen from Fig.5.6, the value of the first sidelobe level is 1.28 dB less than that based on image theory. Also the beamwidth is 0.2° lower. The radiation patterns based on the two methods show good agreement.

The fourth case examined in this chapter is the offset case described in chapter III. The design parameters given in chapter III are used to calculate the radiation pattern. It is found that the lowest main to sidelobe level occurs for a reflector length of 7.1λ.

The radiation pattern corresponding to this case , using the I.E.F method is given in Fig.5.7. The main to sidelobe level is again lower by 2.31 dB than that based on image theory while the beamwidth is almost the same.

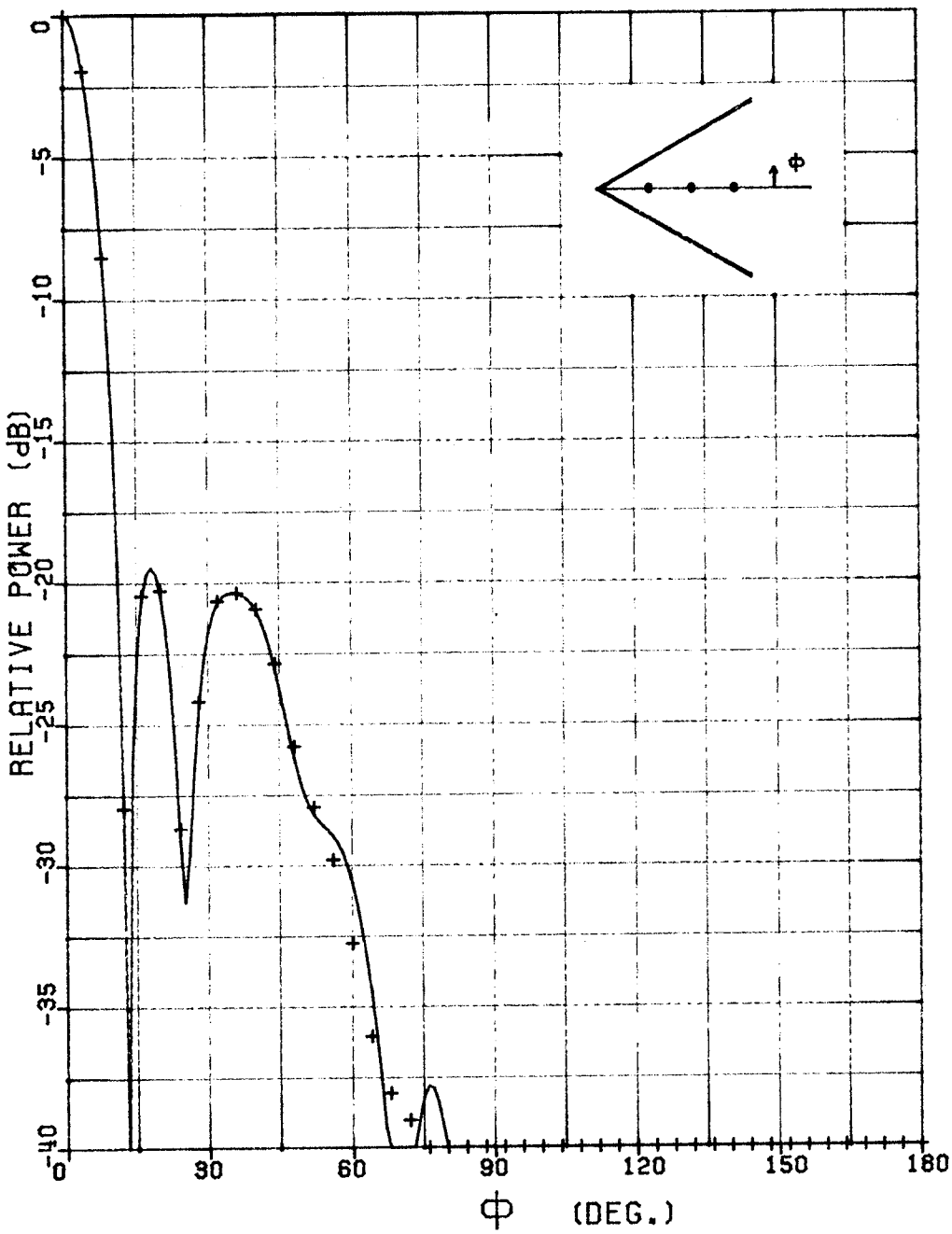

FIG.5.4: RADIATION PATTERN FOR SCHELL CASE

REFLECTOR LENGTH 7.1

—— I.E.F

+++ G.T.D

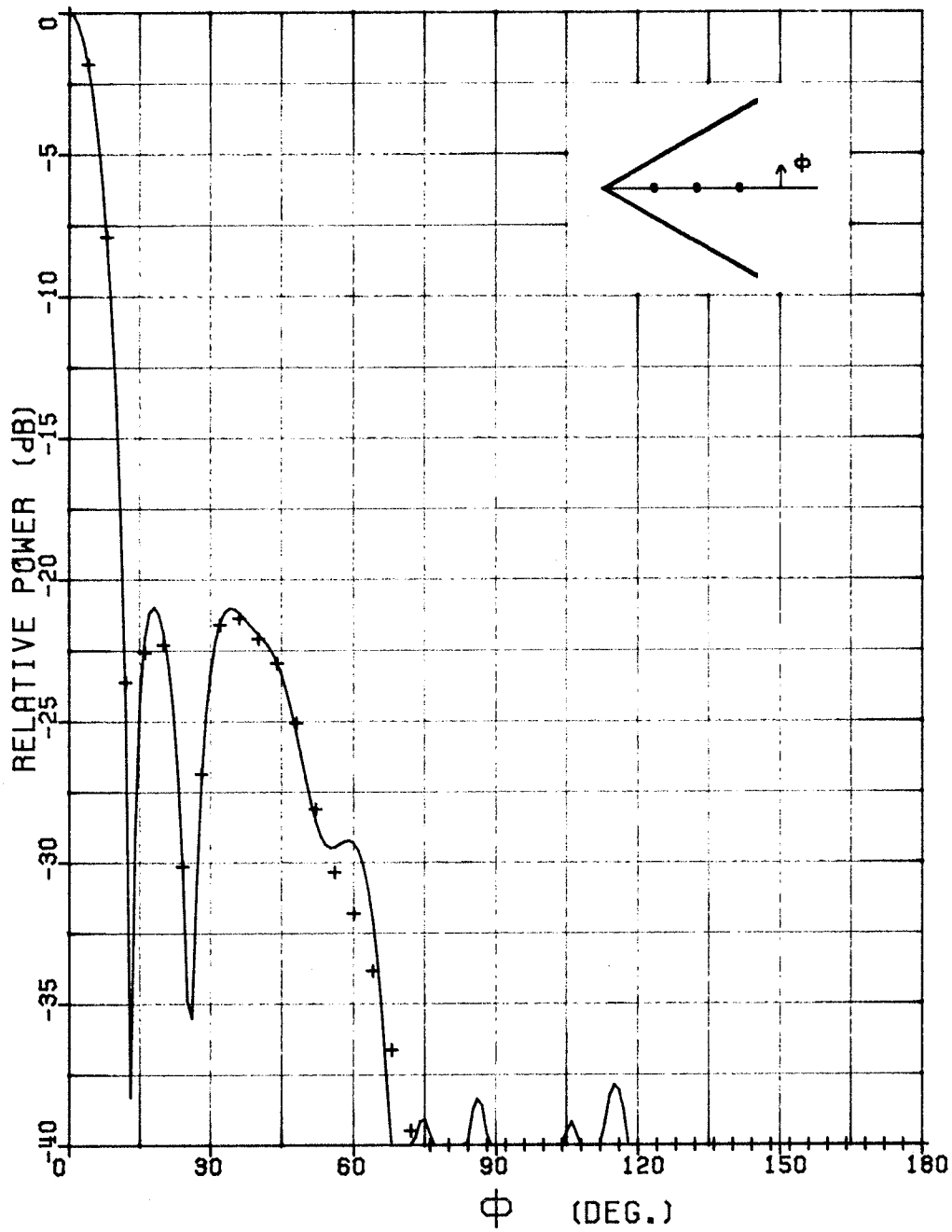

FIG.5.5: RADIATION PATTERN FOR EQUISPACED FEED ARRAY

REFLECTOR LENGTH 6.7

—— I.E.F

+++ G.T.D

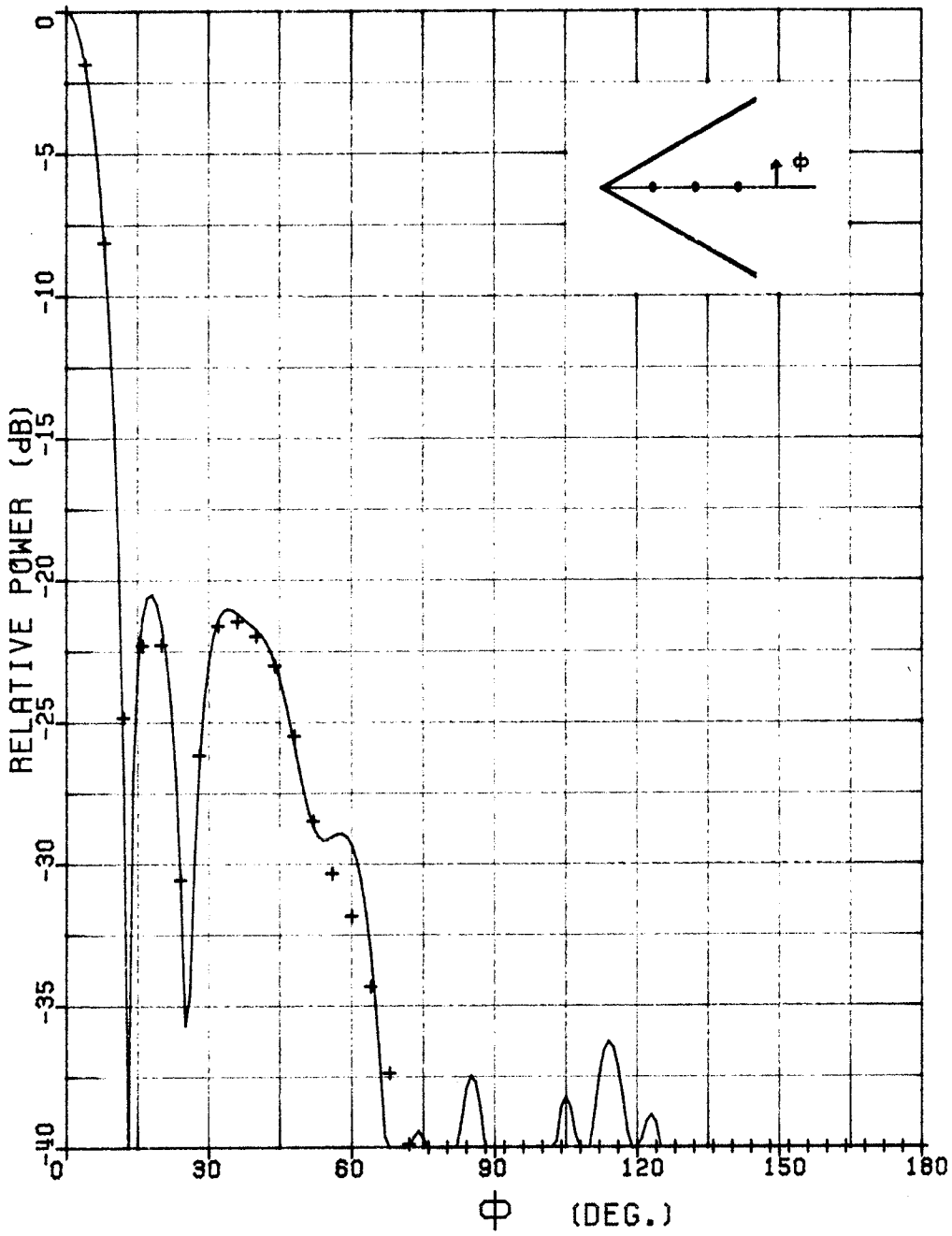

FIG.5.6: RADIATION PATTERN FOR UNEQUISPACED FEED ARRAY

REFLECTOR LENGTH 6.8

—— I.E.F

+++ G.T.D

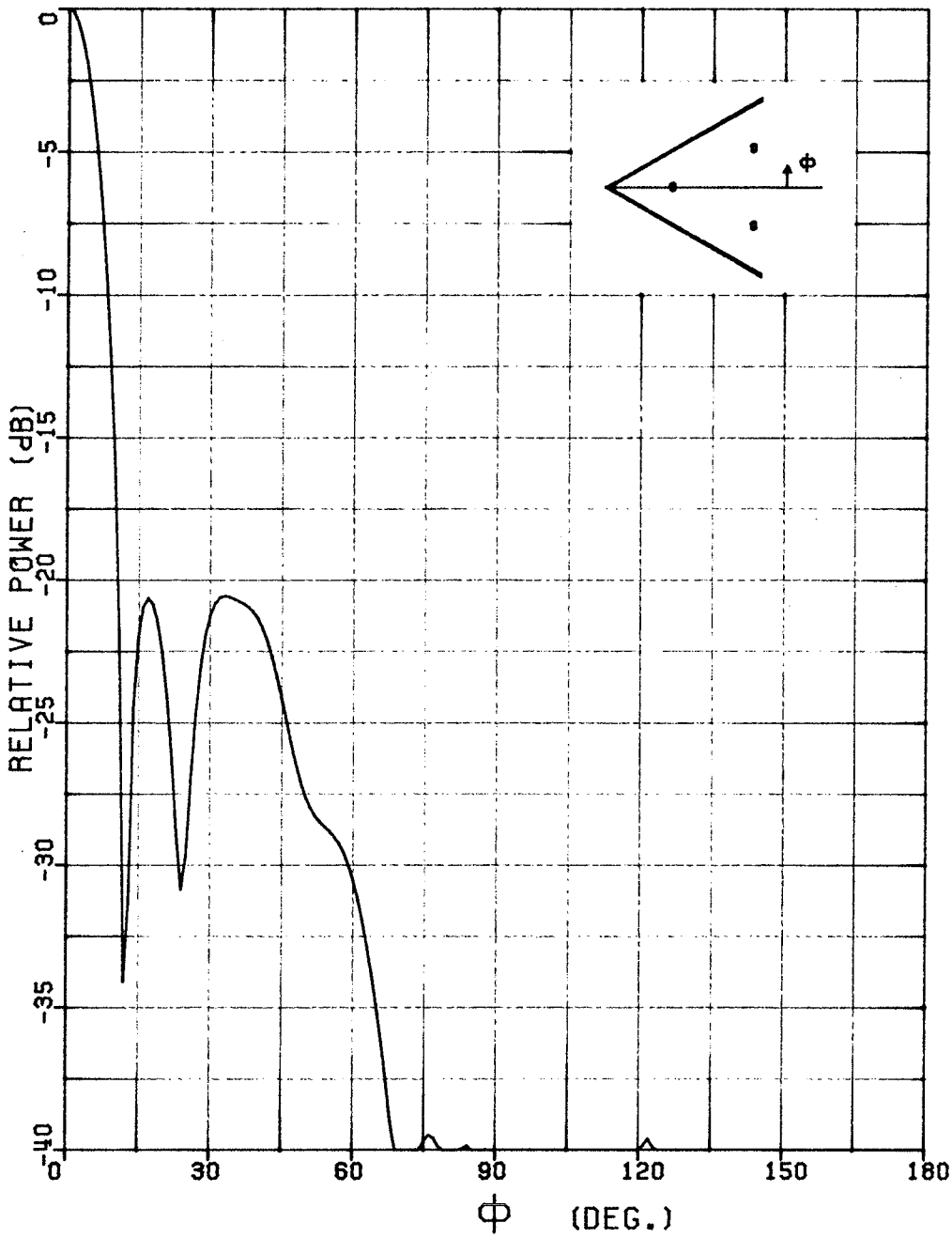

FIG.5.7: RADIATION PATTERN FOR THE OFFSET CASE

REFLECTOR LENGTH 7.1

—— I.E.F

Chapter VI

CONCLUSIONS

6.1 GLOBAL OPTIMUM

An investigation is made throughout this thesis to obtain an optimum design of the corner array. Several effects on the radiation characteristics which were not previously considered are investigated. In each chapter one effect is inserted in the calculation of the radiation characteristics and a numerical procedure is employed to obtain the optimum design. Since each effect is studied separately in each chapter, the optimum designs calculated are only partially optimum. It is therefore obvious that, all effects should be considered simultaneously in the calculation of the corner array characteristics. For this purpose a search program is done, taking into account the effects of the locations as well as mutual coupling and edge diffraction. The main goal of this search is to obtain a global optimum for certain design specifications of the corner array characteristics. For this case, the design specifications are taken as the gain being higher than 19.0 dB with the side to main lobe level less than -20 dB. Since the radiating element locations have a significant effect on the gain and sidelobe level, they are taken as variables in the search program. This search technique is illustrated in the flow chart given in appendix C. The reflector length is fixed at 5.5 λ in the search program,

and after the design parameters are calculated, a slight variation in the length is done in order to obtain a more refined design. The design parameters and the radiation characteristics obtained are shown in Table 6.1.

6.2 CONCLUSIONS

This thesis has confirmed the possibilty of obtaining increased directivity and gain of an ordinary corner reflector antenna by increasing the number of sources within the reflector. The optimum locations of the radiating elements and the application of the Dolphe Tchebyscheff technique to calculate the optimum pattern and gain have been obtained for N radiating elements positioned on or off the axis. The corner angle, which was restricted by Schell to an integral fraction of 180°, has also been made arbitrary to allow further extension to the analysis of the corner array. The practical effects of the element to element coupling and edge diffraction have also been studied.

For the mutual coupling, the current distribution along the feed dipoles has been derived using an approximate method for solving an appropriate integral equation for the magnetic vector potential. The radiation pattern has been calculated using this current distribution. It has been found that the mutual coupling has a significant effect on the main to sidelobe level as well as the beamwidth and gain. This effect is highly dependent on the element to element spacing and excitation currents. For the optimum pattern, the Dolph Tchebyscheff technique has been employed to re-calculate

the values of the driving currents. Also for the optimum gain, the locations are re-calculated and the main to sidelobe level is found to be highly increased. It should be noted that the effect of mutual coupling is beneficial in increasing the gain of the antenna if the radiating elements are correctly located.

For the edge diffraction effect, two methods are used for calculating the pattern. The main effect of the edge diffraction appears in the sidelobes and the beamwidth. As long as the reflector length is infinite or large relative to the wavelength, the pattern is essentially free of sidelobes. However, in practice reflector length is finite and edge diffraction yields a sidelobe outside the geometrical optics region of the antenna. It is found that by increasing the reflector length beyond the minimum value calculated by Schell, the sidelobe level and the beamwidth first decrease and then increase again. The value of the reflector length corresponding to the lowest sidelobe level is calculated for each design case considered. Once an optimum reflector length is found, the sidelobe level is actually below that corresponding to a reflector of infinite length. This suggests that the edge diffraction may be important in decreasing the sidelobe level when the radiating element locations are in specific positions. For a global optimum design, a compromise between the gain and the sidelobe level must be specified by the designer in order to take into account all effects. An example of this case is given in table 6.1 showing that design parameters may be globally optimized with the resulting radiation characteristics still in agreement with the specified values.

It should be pointed out that the 'global' optimum design is by no means optimum since effects such as the coupling between edges and radiating elements has been neglected. Also it might be more useful to base the optimum design on the wall current distribution rather than the far field characteristics. Since the optimum current distribution corresponding to the far field optimum was not specifically calculated, the feasibilty of a such procedure would have to be evaluated with further research.

TABLE 6.1

Design Parameters and Radiation characteristics of Optimum Design (ψ=60°, 3-driven elements)

	Element 1	Element 2	Element 3
$\|I\|$	2.00	0.41	0.28
θ	0.00	-177.0	4.00
ρ/λ	0.25	1.04	2.37
Gain (dB)	19.1		
B.W. (Deg.)	11.0		
R (dB)	21.1		
L/λ	5.8		

Appendix A

CURRENT DISTRIBUTION ALONG THE FEED DIPOLES

The solution of the integral equation (4.39) can be achieved using the approximate method mentioned in section 4.2 . The magnetic potential difference integral equation (4.39) for the Kth feed dipole, where m equals 1, can be written as

$$\int_{-H}^{H} \sum_{i=1}^{N} \sum_{\ell=1}^{2M} I_{zi\ell}(Z') \, K_{ki\ell d}(Z,Z') \, dZ' = \frac{j4\pi}{\eta \cos\beta H} \left[U_k F_{oz} + \tfrac{1}{2} V_{ok} M_{oz} \right] \qquad (A.1)$$

Due to circular symmetry and similar arrangement of the elements around each circle, the current distribution along the 1th dipole in the ith circle can be written as

$$I_{zi\ell}(Z) = (-1)^{\ell-1} \, I_{zi}(Z) \qquad (A.2)$$

substituting (A.2) into (A.1) leads to

$$\int_{-H}^{H} \sum_{i=1}^{N} I_{zi}(Z') \, K_{kid}(Z,Z') \, dZ' = \frac{j4\pi}{\eta \cos\beta H} \left[U_k F_{oz} + \tfrac{1}{2} V_{ok} M_{oz} \right] \qquad (A.3)$$

where

$$U_k = \frac{-j\eta}{4\pi} \int_{-H}^{H} \sum_{i=1}^{N} I_{zi}(Z') \, K_{ki}(H, Z') \, dZ' \qquad (A.4)$$

and where the kernel of the integral equation is given by

$$K_{kid}(Z,Z') = \sum_{\ell=1}^{2M} (-1)^{\ell-1} \, K_{ki\ell d}(Z,Z') \qquad (A.5)$$

the difference kernel may be separated into its real and imaginary parts as

$$K_{kid} = K_{kidR} + j K_{kidI} \tag{A.6}$$

For the single element, the integrals corresponding to those in (A.3) were separated into two groups depending on the manner in which their leading terms varied as function of z [17]. One group varies approximately as M_{oz} and the other as F_{oz} . The following functional forms for the integrals (A.3) are important general criteria for separation:

$$\int_{-H}^{H} I_{zi}(z')\ K_{kiR}(z,z')\ dz' \sim I_{zi}(z) \qquad \text{for} \quad \beta b_{ki} < 1 \tag{A.7}$$

$$\int_{-H}^{H} I_{zi}(z')\ K_{kiR}(z,z')\ dz' \sim F_{oz} \qquad \text{for} \quad \beta b_{ki} \geqslant 1 \tag{A.8}$$

$$\int_{-H}^{H} I_{zi}(z')\ K_{kiI}(z,z')\ dz' \sim F_{oz} \quad , \qquad \text{for all} \quad \beta b_{ki} \tag{A.9}$$

The current in each element can now be expressed as two terms of the form [17]

$$I_{zi}(z) = I_{ui}(z) + I_{vi}(z) \tag{A.10}$$

When (A.10) is substituted into (A.3), groups of integrals occur and may be expressed as follows for all k with i in the range 1 to N

$$\int_{-H}^{H} I_{ui}(z')\ K_{kid}(z,z')\ dz' = \left(\frac{B_i}{B_k}\right) \Psi_{kidu}\ I_{uk}(z) - D_{kidu}(z) \ \text{for all}\ b_{ki} \tag{A.11}$$

$$\int_{-H}^{H} I_{vi}(z')\, K_{kid}(z,z')\, dz' = \left(\frac{jA_i}{B_k}\right) \Psi_{kidv}\, I_{uk}(z) - D_{kidv}(z) \text{ for } \beta b_{ki} \geqslant 1 \quad (A.12)$$

$$\int_{-H}^{H} I_{vi}(z')\, K_{kidR}(z,z')\, dz' = \left(\frac{A_i}{A_k}\right) \Psi_{kidR}\, I_{vk}(z) - D_{kidR}(z) \text{ for } \beta b_{ki} < 1 \quad (A.13)$$

$$\int_{-H}^{H} I_{vi}(z')\, K_{kidI}(z,z')\, dz' = \left(\frac{jA_i}{B_k}\right) \Psi_{kidI}\, I_{uk}(z) - D_{kidI}(z) \text{ for } \beta b_{ki} < 1 \quad (A.14)$$

It is assumed that the functions are defined so that the difference terms $D_{ki}(z)$ are small enough to be negligible in a solution of zero order. The coefficient (jA_i/B_k) in (A.12) is the ratio of the amplitude of I_{vi} (z) to that of I_{uk} (z). In our problem the spacing between the elements are sufficiently large such that $\beta b_{ik} \geqslant 1$ and only $\beta b_{kk} < 1$. In this case, when (A.11) to (A.14) are substituted into (A.3), the following separation into two groups of equations may be carried out

$$I_{vk}(z) = \frac{jz\pi V_{ok}}{\eta\, \Psi_{dR} \cos\beta H}\, M_{oz} \quad (A.15)$$

$$\sum_{i=1}^{N} \left\{ \left(\frac{B_i}{B_k}\right) \Psi_{kidu} + \left(\frac{jA_i}{A_k}\right) \left[\Psi_{kidv}(1-\delta_{ki}) + j(\Psi_{kidI} - j\,\Psi_{kidvI})\,\delta_{ik} \right] \right\}$$

$$= \frac{j4\pi U_k}{\eta \cos\beta H}\, F_{oz} \quad (A.16)$$

The notation Ψ_{dR} equal to Ψ_{kkdR} is used, since for identical elements all the Ψ_{kkdR} are identical and equal to Ψ_{dR}. It follows directly from (A.15) that the leading term in I_{vk} (z) is always M_{oz} for each value of k. similarly from (A.16) the leading term in $I_{uk}(z)$ is of the form F_{oz}. Hence, it is possible to set

$$I_{zi}(z) = jA_i\, M_{oz} + B_i F_{oz} \quad (A.17)$$

Since Ψ_{dR} is real, it is clear from (A.15) that A_i is real when V_{ok} is real and from (A.16) that B_i is in general complex. With the zero-order current formally determined, the constant U_k may be obtained from the substitution of (A.17) in (A.4) which gives

$$U_k = -j\frac{\eta}{4\pi}\sum_{i=1}^{N}\left[jA_i\,\Psi_{kiv}(H) + B_i\,\Psi_{kiu}(H)\right] \tag{A.18}$$

where

$$\Psi_{kiv}(H) = \int_{-H}^{H} M_{oz'}\;K_{ki}(H,z')\,dz' \tag{A.19}$$

$$\Psi_{kiu}(H) = \int_{-H}^{H} F_{oz'}\;K_{ki}(H,z')\,dz' \tag{A.20}$$

If (A.18) and (A.17) are substituted in (A.15) and (A.16) the result is

$$A_k = \frac{2\pi}{\eta\,\Psi_{dR}\cos\beta H}\;V_{ok} \tag{A.21}$$

$$\sum_{i=1}^{N} B_i\left[\Psi_{kidu}\cos\beta H - \Psi_{kiu}(H)\right] = j\sum_{i=1}^{N} A_i\Big\{\Psi_{kiv}(H) - \left[\Psi_{kidv}(1-\delta_{ik}) + j\left(\Psi_{kidf} - j\Psi_{kidvi}\right)\delta_{ik}\right]\cos\beta H\Big\} \tag{A.22}$$

where k=1,2,------,N

The physical significance of the zero-order solution is evident from (A.21) and (A.22). The coefficients of the transmitting part of the current are given by (A.21). The driving voltages generate the expected sinusoidal distribution of current on each element.

The coefficients of the receiving part of the current are given by (A.22). Equation (A.22) permits the prediction in each driven element of the shifted-cosine component of the current that is due to coupling between currents distributed along the element itself and along all other elements in the array. Equation (A.22) is a set of linear algebraic equations with N unknowns which may be solved for B_i in terms of A_i. The N values of the A_i are expressed in terms of the N driving voltages V_{ok} by (A.21). In order to express (A.22) in matrix form, let the following quantities be defined

$$\Phi_{kiu} = \Psi_{kidu} \cos\beta H - \Psi_{kiu}(H) \tag{A.23}$$

$$\Phi_{kiv} = \Psi_{kiv}(H) - \Psi_{kidv} \cos\beta H (1-\delta_{ik}) - j(\Psi_{kidI} - j\Psi_{kidvI})\,\delta_{ik} \cos\beta H \tag{A.24}$$

From (A.23) and (A.24) equation (A.22) can be written as

$$[\Phi_u]\{B\} = [\Phi_v]\{jA\} \tag{A.25}$$

Thus the vector {B} can be written as

$$\{B\} = [\Phi_u]^{-1}[\Phi_v]\{jA\} \tag{A.26}$$

The general $\Psi(z)$ functions obtained from the defining integrals are

$$\Psi_{kidu}(z) = (\cos\beta z - \cos\beta H)^{-1}\left\{[C_{bi}(H,z) - C_{bi}(H,H)] - \cos\beta H\,[E_{bi}(z) - E_{bi}(H,H)]\right\} \tag{A.27}$$

$$\Psi_{kidR}(z) = (\sin\beta(H-|z|))^{-1}\,\mathrm{Re}\left\{[C_{bi\Sigma I}(H,z) - C_{bi\Sigma I}(H,H)]\sin\beta H - [S_{bi\Sigma I}(H,z) - S_{bi\Sigma I}(H,H)]\cos\beta H\right\} \tag{A.28}$$

$$\Psi_{kidI}(z) = (\cos\beta z - \cos\beta H)^{-1}\,\mathrm{Im}\left\{[C_{bi\Sigma I}(H,z) - C_{bi\Sigma I}(H,H)]\sin\beta H - [S_{bi\Sigma I}(H,z) - S_{bi\Sigma I}(H,H)]\cos\beta H\right\} \tag{A.29}$$

$$\Psi_{kidv}(Z) = (\cos\beta Z - \cos\beta H)^{-1}\left\{\left[C_{bi}(H,Z) - C_{bi}(H,H)\right]\sin\beta H - \left[S_{bi}(H,Z) - S_{bi}(H,H)\right]\cos\beta H\right\} \quad (A.30)$$

$$\Psi_{kidvl}(Z) = (\cos\beta Z - \cos\beta H)^{-1}\left\{\left[C_{bi\Sigma 2}(H,Z) - C_{bi\Sigma 2}(H,H)\right]\sin\beta H - \left[S_{bi\Sigma 2}(H,Z) - S_{bi\Sigma 2}(H,H)\right]\cos\beta H\right\} \quad (A.31)$$

$$\Psi_{kiv}(H) = C_{bi}(H,H)\sin\beta H - S_{bi}(H,H)\cos\beta H \quad (A.32)$$

$$\Psi_{kiu}(H) = C_{bi}(H,H) - E_{bi}(H,H)\cos\beta H \quad (A.33)$$

$$S_{bi}(H,Z) = \sum_{\ell=1}^{2M}(-1)^{\ell-1} S_{bi\ell} \quad ; \quad S_{bi\ell}(H,Z) = \int_0^H \sin\beta Z'\left[\frac{e^{-j\beta R_1}}{R_1} + \frac{e^{-j\beta R_2}}{R_2}\right] dZ' \quad (A.34)$$

$$E_{bi}(H,Z) = \sum_{\ell=1}^{2M}(-1)^{\ell-1} E_{bi\ell} \quad ; \quad E_{bi\ell}(H,Z) = \int_0^H \left[\frac{e^{-j\beta R_1}}{R_1} + \frac{e^{-j\beta R_2}}{R_2}\right] \quad (A.35)$$

$$C_{bi}(H,Z) = \sum_{\ell=1}^{2M}(-1)^{\ell-1} C_{bi\ell} \quad , \quad C_{bi\ell}(H,Z) = \int_0^H \cos\beta Z'\left[\frac{e^{-j\beta R_1}}{R_1} + \frac{e^{-j\beta R_2}}{R_2}\right] dz' \quad (A.36)$$

$$R_1 = \sqrt{(Z-Z')^2 + b_{ki\ell}^2} \quad , \quad R_2 = \sqrt{(Z+Z')^2 + b_{ki\ell}^2} \quad (A.37)$$

Where the subscript $\Sigma 1$ indicates that only element number 1 in the Kth circular array is to be included while the subscript $\Sigma 2$ indicates that only the effect of elements other than element number 1 are to be included. For the special case of βH equal to $\pi/2$ the expression of the current distribution becomes indeterminate of the form 0/0, so that the formula for the current may be rearranged as

$$\{I_z(z)\} = \frac{-z\pi j}{\eta \Psi_{dR}} \left[\{V_o\} \left(\sin\beta|z| - 1 \right) + [\Phi_u']^{-1} [\Phi_v'] \{V_o\} \cos\beta z \right] \quad (A.38)$$

where

$$\Phi'_{kiu} = \Psi_{kiu}(H) \quad (A.39)$$

$$\Phi'_{kiv} = \Psi_{kidu} - \Psi_{kidv}(1 - \delta_{ik}) - j\left(\Psi_{kidI} - j\Psi_{kidvI} \right) \delta_{ik} \quad (A.40)$$

Appendix B

FAR FIELD RADIATION PATTERN

The whole space is divided into 22 regions as shown in Fig.5.3. Since the dipole is located on the bisector of the corner angle, there is a symmetry between the regions above and below the axis. In this case it is sufficient to calculate the radiation pattern in regions 1 to 12. The results obtained for the far fields pattern are given below.

In region 2

$$\frac{E}{E_c} = \sum_{\ell=1}^{N} \left\{ I_\ell \sum_{n=1}^{6} (-1)^{n-1} e^{j\beta S_\ell \cos(\phi-(n-1)\frac{\pi}{3})} F_2^{(\ell)}(n) \right\} \tag{B.1}$$

where

$$F_2^{(\ell)}(n) = 1 - \tfrac{1}{2}\left\{ X(T_{nA}^{(\ell)}) + X(T_{nB}^{(\ell)}) + X(T_{nB2}^{(\ell)}) \right\} \tag{B.2}$$

In region 3

$$\frac{E}{E_c} = \sum_{\ell=1}^{N} \left\{ I_\ell \sum_{\substack{n=1 \\ n\neq 3}}^{6} (-1)^{n-1} e^{j\beta S_\ell \cos(\phi-(n-1)\frac{\pi}{3})} F_2^{(\ell)}(n) + e^{j\beta S_3 \cos(\phi-\frac{2\pi}{3})} F_4^{(\ell)}(3) \right\} \tag{B.3}$$

where

$$F_4^{(\ell)}(3) = \tfrac{1}{2}\left\{ X(T_{3A}^{(\ell)}) - X(T_{3B}^{(\ell)}) - X(T_{3B2}^{(\ell)}) \right\} \tag{B.4}$$

In region 4

$$\frac{E}{E_c} = \sum_{\ell=1}^{N} \left\{ I_\ell \sum_{\substack{n=1 \\ n\neq 2,3}}^{6} (-1)^{n} e^{j\beta S_\ell \cos(\phi-(n-1)\frac{\pi}{3})} F_2^{(\ell)}(n) + \sum_{i=2,3} (-1)^{i-1} e^{j\beta S_\ell \cos(\phi-(i-1)\frac{\pi}{3})} F_4(i) \right\} \tag{B.5}$$

In region 5

$$\frac{E}{E_c} = \sum_{\ell=1}^{N} I_\ell \left\{ \sum_{\substack{n=1 \\ odd}}^{6} (-1)^{n-1} e^{j\beta S'_\ell \cos(\phi-(n-1)\frac{\pi}{3})} F_2^{(\ell)}(n) + \sum_{\substack{i=2 \\ even}}^{6} (-1)^{i-1} e^{j\beta S'_\ell \cos(\phi-(i-1)\frac{\pi}{3})} F_4^{(\ell)}(i) \right\} \quad (B.6)$$

In region 6

$$\frac{E}{E_c} = \sum_{\ell=1}^{N} I_\ell \left\{ \sum_{\substack{n=1 \\ n\neq 2,3,4}}^{6} (-1)^{n-1} e^{j\beta S'_\ell \cos(\phi-(n-1)\frac{\pi}{3})} F_5^{(\ell)}(n) + \sum_{i=2}^{4} (-1)^{i-1} e^{j\beta S'_\ell \cos(\phi-(i-1)\frac{\pi}{3})} F_6^{(\ell)}(i) \right\} \quad (B.7)$$

where

$$F_5(n) = 1 - \tfrac{1}{2}\left\{ X(T_{nA}) + X(T_{nB}) + X(T_{nA1}) \right\} \quad (B.8)$$

$$F_6(i) = \tfrac{1}{2}\left\{ X(T_{iA}) - X(T_{iB}) - X(T_{iA1}) \right\} \quad (B.9)$$

In region 7

$$\frac{E}{E_c} = \sum_{\ell=1}^{N} I_\ell \left\{ \sum_{n=1,6} (-1)^{n-1} e^{j\beta S'_\ell \cos(\phi-\frac{\pi}{3})} F_5^{(\ell)}(6) + \sum_{i=2}^{5} (-1)^{i-1} e^{j\beta S'_\ell \cos(\phi-(i-1)\frac{\pi}{3})} F_6^{(\ell)}(i) \right\} \quad (B.10)$$

In region 8

$$\frac{E}{E_c} = \sum_{\ell=1}^{N} I_\ell \left\{ -e^{j\beta S'_\ell \cos(\phi-\frac{5\pi}{3})} F_5^{(\ell)}(6) + \sum_{i=1}^{5} (-1)^{i-1} e^{j\beta S'_\ell \cos(\phi-(i-1)\frac{\pi}{3})} F_6^{(\ell)}(i) \right\} \quad (B.11)$$

In region 9

$$\frac{E}{E_c} = \sum_{\ell=1}^{N} I_\ell \left\{ \sum_{n=1}^{6} (-1)^{n-1} e^{j\beta S'_\ell \cos(\phi-(n-1)\frac{\pi}{3})} F_7^{(\ell)}(n) \right\} \quad (B.12)$$

where

$$F_7^{(\ell)}(n) = \tfrac{1}{2}\left\{ X(T_{nA}^{(\ell)}) - X(T_{nB}^{(\ell)}) + X(T_{nA1}^{(\ell)}) \right\} \quad (B.13)$$

In region 10

$$\frac{E}{E_c} = \sum_{\ell=1}^{N} I_\ell \left\{ \sum_{n=1}^{6} (-1)^{n-1} e^{j\beta S'_\ell \cos(\phi-(n-1)\frac{\pi}{3})} F_8^{(\ell)}(n) \right. \quad (B.14)$$

where

$$F_g(n) = \tfrac{1}{2}\left\{ X(T_{nA}^{(\ell)}) - X(T_{nB}^{(\ell)}) \right\} \tag{B.15}$$

In region 11

$$\frac{E}{E_c} = \tfrac{1}{2} \sum_{\ell=1}^{N} I_\ell \left\{ \sum_{n=1}^{6} (-1)^{n-1} \; e^{j\beta S'_\ell \cos(\phi - (n-1)\frac{\pi}{3})} \; X(T_{nA}^{(\ell)}) \right. \tag{B.16}$$

In region 12

$$\frac{E}{E_c} = \sum_{\ell=1}^{N} I_\ell \left\{ \sum_{n=1}^{6} (-1)^{n-1} \; e^{j\beta S'_\ell \cos(\phi - (n-1)\frac{\pi}{3})} \; F_g^{(\ell)}(n) \right. \tag{B.17}$$

where

$$F_g^{(\ell)}(n) = \tfrac{1}{2}\left\{ X(T_{nA}^{(\ell)}) + X(T_{nB}^{(\ell)}) \right\} \tag{B.18}$$

Appendix C

FLOW CHART

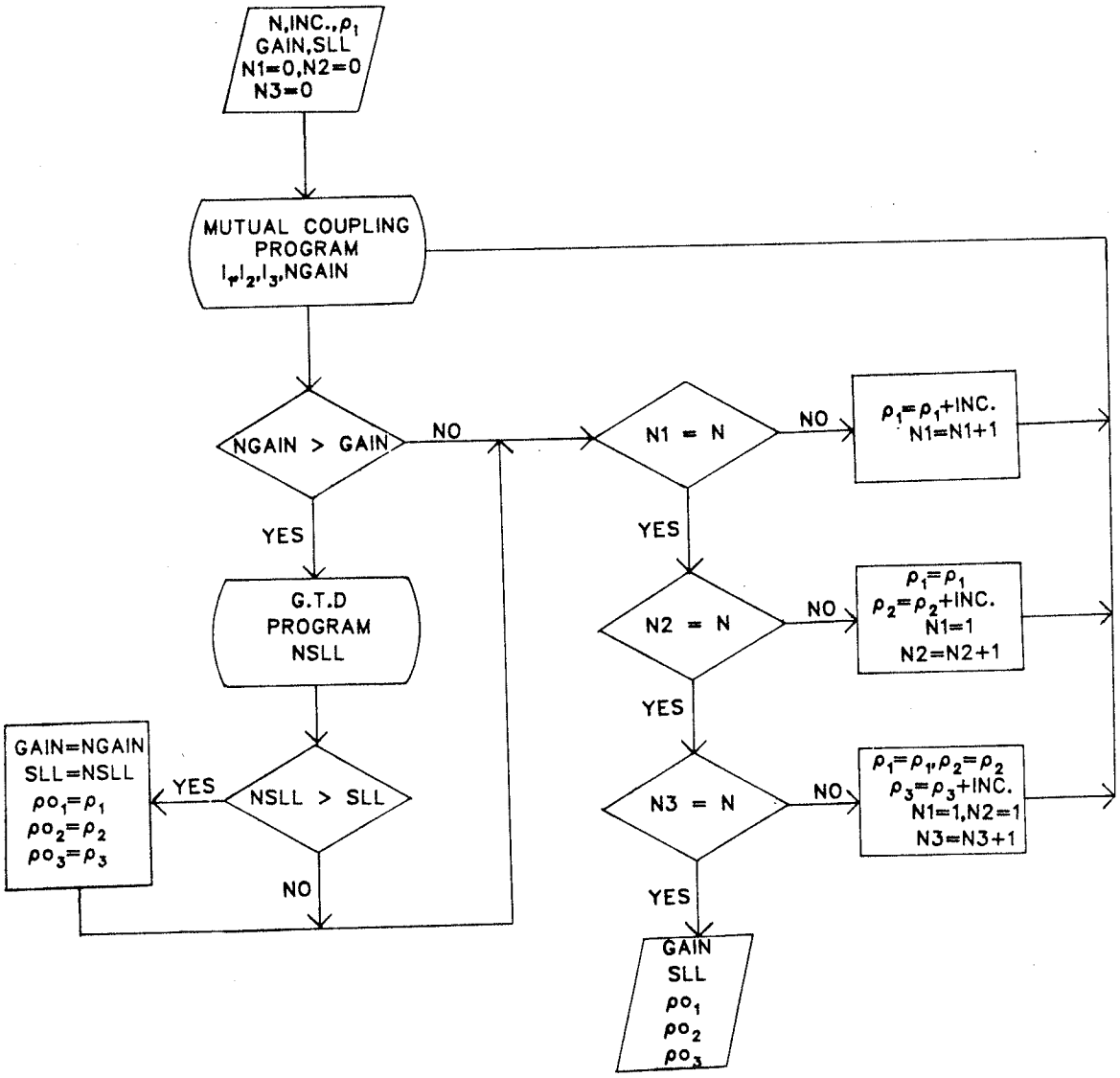

REFERENCES

1. D. Kraus,'The Corner Reflector Antenna',Proc. IRE Vol. 28, P.513, November 1940 .

2. E. B. Moullin,'Theory and Performance of Corner Reflector for Aerials', J. Inst. Elec. Engrs. Pt. III, Vol. 92, PP. 58-67, 1945.

3. J. R. Wait,'On the Theory of an Antenna With an Infinite Corner Reflector', Can. J. of Phys., Vol. 32, PP. 365-371, May 1954.

4. R. W. Klopfenstein,'Corner Reflector Antennas With Arbitrary Dipole Orientation', Proc. IRE

5. H. P. Neff and J. D. Tillman,'The Design of the Corner Reflector Antenna', Communication and Electronics. No. 43, PP. 293-295, July 1959.

6. Y. Ohba,'On the Radiation Pattern of a Corner Reflector Finite in Width' , IEE Trans. Ant. and Prop., AP-11, PP. 127-132, March 1960.

7. A. C. Wilson and H. V. cottony,'Radiation Pattern of Finite-Size Corner Reflector Antenna', IRE Trans. Ant and Prop. , AP-8, PP. 144-157, March 1960

8. A. C. Wilson and H. V. Cottony,'Gains of Finite-Size Corner Reflector Antenna',IRE Trans. Ant. and Prop., AP-6, PP. 366-396, October,1958

9. L. L. Tasi, D. R. Wilton, M. G. Harrison, and E. H. Wright,'A Comarison of Geometrical Therory OF Diffraction And Integral Equation Formulation For Analysis of Reflector Antennas', IEEE Trans. and Prop., AP-20, PP. 705-712, November 1972

10. R. W. Redlich,'Approximate Method of Calculating The Radiation Pattern of A Corner Reflector Antenna', Proc. IEE, Vol. 121 , No. 8, PP. 805-806, August 1974

11. T. Kilsuregawa, Y. Takeichi and M. Mizusawa,'offset Dipole Corner Reflector Antenna', Mitsubishi Denki Laboratory Reports, PP. 145-157, April 1965

12. A. Z. El-sherbeni,'Critical Survey of The Analysis of Corner Reflector Antennas', M.Sc. thesis, Facultiy of Eng., Cairo University, Egypt 1982

13. H. M. Elkamchouchi,'Cylindrical and Three-Dimensional Corner Reflector Antennas',IEEE Trans. Antennas and Propagation., Vol. AP-31, No. 3, PP. 451-455, June, 1983 .

14. A. C. Schell,' The Corner Array', Air Force Cambridge Research Center, Bedford, Mass., TR-59-105, January, 1959

15. C. L. Dolph,'A Current Distribution for Broadside Array which Optimizes the Relationship between Beamwidth and sidelobe level',Proc. IRE, 34(1946), 335-348.

16. M. Abramowitz and I. A. Stegum,'Handbook OF Mathematical Tables', June 1964,PP. 355-445

17. R. W. King, R. B. Mack and S.S. Sandler,'Arrays of Cylindrical Dipoles', Cambridge, at the University press, 1968

18. L. V. King,'On The Radiation Field of A Perfectly Conducting Base Insulated Cylindrical Antenna Over A Perfectly Conducting Plane Earth, and The Calculation of Radiation Resistance and Reactance', Trans. Roy. Soc(London) (A) 236, 1937, P. 381.

19. E. Hallen,'On Antenna Impedance',Acta ploytech. No. 16-Trans Roy. Inst. Technol. Stockholm, 1947

20. S.A. Schelkunoff,'Theroy of Antenna of Arbitrary Shape And Size', Proc. IRE, Vol. 29, 1941, P.511

21. H. C. Polklington,'Electric Oscillations In Wires',Camb. Phil. Soc., 9, 1897, P.324

22. R. King and D. Middleton,'The Thin Cylindrical Antenna, A Comparison of Theories',J. Appl. Physics, Vol. 17, 1946, P.273

23. R. F. Harrington,'Time-Harmonic Electromagnetic Fields', McGraw-Hill, New York, 1961

24. G. L. James,'Geometrical Theory of Diffraction for Electromagnetic Waves', Peter Peregrinus, London, 1980.

25. R. F. Harrington,'Field Comutation by Moment Methods', Macmillan, New York, P. 58, 1960